

## Theory of magnetic deflagration in crystals of molecular magnets

D. A. Garanin and E. M. Chudnovsky

*Department of Physics and Astronomy, Lehman College, City University of New York,  
250 Bedford Park Boulevard West, Bronx, New York 10468-1589, USA*

(Received 25 April 2007; published 6 August 2007)

Theory of magnetic deflagration (avalanches) in crystals of molecular magnets has been developed. The phenomenon resembles the burning of a chemical substance, with the Zeeman energy playing the role of the chemical energy. Nondestructive reversible character of magnetic deflagration, as well as the possibility to continuously tune the flammability of the crystal by changing the magnetic field, makes molecular magnets an attractive toy system for a detailed study of the burning process. Besides simplicity, new features, as compared to the chemical burning, include possibility of quantum decay of metastable spin states and strong temperature dependence of the heat capacity and thermal conductivity. We obtain analytical and numerical solutions for criteria of the ignition of magnetic deflagration and compute the ignition rate and the speed of the developed deflagration front.

DOI: [10.1103/PhysRevB.76.054410](https://doi.org/10.1103/PhysRevB.76.054410)

PACS number(s): 75.50.Xx, 76.60.Es, 82.33.Vx

### I. INTRODUCTION

Recently, it has been observed that molecular magnets exhibit explosive relaxation toward thermal equilibrium that resembles propagation of a flame through a flammable chemical substance.<sup>1</sup> Theory of this effect is the subject of this paper.

Crystals of molecular magnets first attracted the attention of physicists after it was demonstrated<sup>2</sup> that individual molecules inside such crystals behave as superparamagnetic particles.<sup>3</sup> Due to large molecular spin (e.g.,  $S=10$  for  $\text{Mn}_{12}$  and  $\text{Fe}_8$  molecular magnets) and high magnetic anisotropy, spin-up and spin-down states of many molecular magnets are separated by a large energy barrier. Consequently, unlike conventional paramagnets, molecular magnets are characterized by a macroscopic time of thermal relaxation between spin-up and spin-down states. Similarly, large times are needed for quantum transitions between these states to occur, which allows one to speak about quantum tunneling of the magnetic moment.<sup>4</sup> Due to this effect, molecular magnets exhibit spectacular staircase magnetization curve.<sup>5</sup> It has been known for some time that the low-temperature magnetic relaxation in crystals of molecular magnets can occur via two mechanisms. The first, slow mechanism involves random thermal and quantum spin transitions at unrelated spatial points. Such transitions influence each other only through weak long-range dipolar fields associated with the magnetic moments of the molecules.<sup>6</sup> The resulting relaxation lasts macroscopic times. This allows one to study transition rates by simply measuring the time dependence of the macroscopic magnetization of the crystal.

The second mechanism of relaxation—magnetic avalanches—corresponds to the abrupt reversal of the magnetization when a sufficiently large crystal is placed in a large magnetic field opposite to its magnetic moment.<sup>7–9</sup> The typical power release in a millimeter sample is in the milliwatt range. The avalanche was long believed to be a thermal runaway in which the Zeeman energy released by the relaxing molecules gets transformed into heat that generates transitions in the neighboring molecules and accelerates the total

energy release. Such a relaxation that typically occurs in a millisecond time was long considered a nuisance as it often interfered with experimental studies of spin tunneling. More recently, it was realized through time-resolved local measurements<sup>1</sup> that magnetic avalanches resemble propagation of a flame—deflagration—in which the role of the chemical energy stored in a flammable substance is played by the Zeeman energy. Due to quantum tunneling between spin states that occurs at discrete values of the magnetic field, magnetic deflagration also exhibits quantum features.<sup>10</sup> Note that, in principle, spins in molecular magnets can reverse collectively through a coherent radiation of phonons similar to the coherent radiation of photons in a laser.<sup>11</sup> On the contrary, magnetic deflagration is a generically incoherent effect as it involves heat conduction carried out by incoherent thermal phonons.

Experiments performed to date have established with certainty that magnetic avalanches in crystals of molecular magnets correspond to the propagation of a narrow front of the magnetization reversal. This should not be confused with the propagation of a domain wall and Barkhausen jumps in magnetic systems having long-range spin order, since exchange interaction between spin clusters in crystals of molecular magnets is typically negligible. The analogy with burning of a flammable chemical substance has been confirmed by the study of the dependence of the flame speed on the energy barrier. In crystals of molecular magnets, the latter can be continuously tuned by the magnetic field. For the study of deflagration, this tunability of the barrier, as well as the reversible nature of the magnetic burning, provides a great advantage over irreversible burning of a chemical substance with a fixed energy barrier. Thus, a detailed study of magnetic deflagration can answer important questions of the theory of combustion and detonation.<sup>12</sup> There are also novel features that are absent in conventional combustion. They include a very strong temperature dependence of the specific heat and thermal conductivity of molecular magnets at low temperature<sup>13–15</sup> and the possibility of magnetization reversal via quantum tunneling.

In this paper we intend to answer the following questions:

(1) the critical combination of parameters (magnetic field,

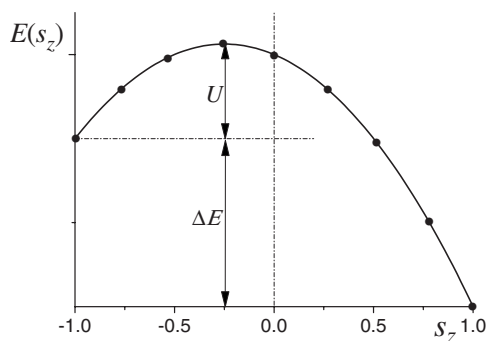


FIG. 1. Energy of a molecular magnet as function of  $s_z$ . Quantum energy levels are shown by black circles for  $S=4$ .

initial temperature, and the size of the sample) that sets off the deflagration process, (2) the mode of instability, (3) the time that elapses between bringing the system above the deflagration threshold and the ignition of the deflagration process (the ignition time), and (4) the temperature of the flame and the velocity of the deflagration front.

We will show that the ignition of magnetic deflagration in molecular magnets is very different from the ignition of magnetization reversal in ferromagnets. The latter is dominated by the exchange interaction and begins with the nucleation of a small critical nucleus of opposite magnetization that spreads and occupies the entire sample. On the contrary, the magnetic deflagration in a paramagnetic crystal of magnetic molecules begins as a large-scale instability of a smooth temperature profile inside the sample against formation of a rapidly moving deflagration front.

The structure of the paper is as follows. Properties of molecular magnets will be discussed in Sec. II. The mechanism of thermal runaway in a crystal of magnetic molecules will be analyzed in Sec. III. Stability of the quasistationary temperature profile in a crystal of molecular magnets will be analyzed in Sec. IV. The ignition rate will be studied in Sec. V. Structure and the velocity of a developed deflagration front will be investigated in Sec. VI. Numerical illustrations of the deflagration process will be given in Sec. VII. Relevance of our results to experiment and possible future directions of theory and experiment will be discussed in Sec. VIII.

## II. MOLECULAR MAGNETS

### A. Magnetic bistability and spin tunneling

A single molecule of a molecular magnet can be described by the Hamiltonian

$$\mathcal{H} = -DS_z^2 - g\mu_B H_z S_z + \mathcal{H}', \quad (1)$$

where  $S$  is spin,  $D$  is the constant of the uniaxial  $z$  anisotropy that creates magnetic bistability,  $H_z$  is the bias magnetic field, and  $\mathcal{H}'$  is a small part of the Hamiltonian that does not commute with  $S_z$  and is responsible for spin tunneling. If  $S$  is large (as, e.g., in  $\text{Mn}_{12}$  and  $\text{Fe}_8$ ), magnetic bistability can be reasonably well described within the classical model with the energy that depends on the classical vector  $\mathbf{s}=\mathbf{S}/S$  and has the form

$$E = -(s_z^2 + 2hs_z)U_0. \quad (2)$$

Here,

$$U_0 = DS^2, \quad h \equiv \frac{g\mu_B H_z}{2DS} \quad (3)$$

are the zero-bias energy barrier and the reduced bias field. The dependence  $E(s_z)$  is shown in Fig. 1. The spin-projection value corresponding to the barrier between the two wells follows from  $dE/ds_z=0$  and is given by  $s_z^{(b)}=-h$ . The minima of  $E$  and its value at the top of the barrier are

$$E_{\pm} = -(1 \pm 2h)U_0, \quad E_b = h^2 U_0. \quad (4)$$

Thus, the values of the energy barriers for the molecules on the left and on the right are given by  $U_{\pm}=E_b-E_{\pm}=(1\pm h)^2 U_0$ . In the case of  $h>0$  that we will consider throughout the paper,  $s_z=-1$  is a metastable minimum, whereas  $s_z=1$  is the absolute minimum of the energy. Below we will use  $U_- \equiv U$ ,

$$U = (1-h)^2 U_0. \quad (5)$$

The energy difference between the two minima is given by

$$\Delta E = E_- - E_+ = 4hU_0. \quad (6)$$

The noncommuting term  $\mathcal{H}'$  in Eq. (1) gives rise to resonance spin tunneling between the states at the two sides of the barrier if the bias field satisfies the condition

$$g\mu_B H_z = kD, \quad k = 0, \pm 1, \pm 2, \dots \quad (7)$$

This modifies the process of thermal activation of spins at low temperatures. Off resonance, the spins have to be thermally activated all the way up from the bottom of the metastable well to the top of the barrier. On resonance, however, it is sufficient to be thermally activated up to the energy level below the barrier where spin tunneling is sufficiently strong to take the molecule to the other side of the barrier. This leads to the resonance increase of the relaxation rate, see Fig. 7 of Ref. 16. On the phenomenological level, this effect can be encapsulated into the effective barrier with dips at the resonance bias fields given by Eq. (7). Since the exact form of the effective barrier depends on the form of  $\mathcal{H}'$  that we do not analyze in this paper, we will use for numerical work the fitting function taken from experiments<sup>9,17</sup> on  $\text{Mn}_{12}$  and replace Eq. (5) by  $U(h)=u(h)U_0$  with

$$u(h) = (1-h)^2 - 0.0806 \left[ 1 - \left| \sin \left( \pi \frac{g\mu_B H_z}{D} \right) \right| \right]^2. \quad (8)$$

Note that in existing experiments, magnetic avalanches always occur above some critical field that greatly exceeds dipole-dipole interactions between magnetic molecules. In that field range, one can safely ignore the effect of dipolar interactions on the energy barrier.

### B. Magnetic relaxation and heat transfer

At low temperatures,

$$\frac{U}{k_B T} \equiv W \gg 1, \quad (9)$$

thermally activated transition of magnetic molecules over the barrier can be described by the rate equations for the numbers of molecules in the left and right wells,  $n_{\pm}$ , that satisfy  $n_+ + n_- = 1$ . The equation for the number of particles in the metastable well  $n_-$  has the form

$$\dot{n}_- = \Gamma_{-+} n_+ - \Gamma_{+-} n_- = -\Gamma [n_- - n_-^{(\text{eq})}], \quad (10)$$

where  $\Gamma = \Gamma_{+-} + \Gamma_{-+}$ . In accordance with the detailed-balance condition,

$$\frac{\Gamma_{+-}}{\Gamma_{-+}} = \frac{n_+^{(\text{eq})}}{n_-^{(\text{eq})}} = \exp\left(\frac{\Delta E}{k_B T}\right), \quad n_-^{(\text{eq})} = \frac{1}{\exp\left(\frac{\Delta E}{k_B T}\right) + 1}. \quad (11)$$

Using  $\Gamma_{+-} = \Gamma_0 e^{-W}$  for  $W \gg 1$ , one obtains

$$\Gamma = \Gamma_0 e^{-W} \left[ 1 + \exp\left(-\frac{\Delta E}{k_B T}\right) \right], \quad (12)$$

where the second term in square brackets describes transitions from the stable well to the metastable well. In the strong-bias case,  $\Delta E \gg k_B T$ , this term can be omitted. This yields simply  $\Gamma = \Gamma_0 e^{-W}$  and sets  $n_-^{(\text{eq})} = 0$  (full burning).

When a magnetic molecule makes a transition from the metastable state  $s_z = -1$  to the absolute energy minimum  $s_z = 1$ , the energy  $\Delta E$  is released. Thermalization of this energy leads to the temperature change  $\Delta T = \Delta E / C_{\text{ph}}$ , where  $C_{\text{ph}}$  is the phonon heat capacity per magnetic molecule. Other contributions to the specific heat at low temperatures are considered small. The magnetic relaxation creates a source in the heat-conduction equation. Another term in this equation is the divergence of the heat flow,

$$\mathbf{q} = -k \nabla T, \quad (13)$$

where  $k$  is thermal conductivity. The full system of equations for the temperature  $T$  and the population of the metastable minimum  $n_-$  has the form

$$\begin{aligned} \frac{\partial T}{\partial t} &= \frac{1}{C_{\text{ph}}} \nabla \cdot k \nabla T - \frac{\Delta E}{C_{\text{ph}}} \frac{\partial n_-}{\partial t}, \\ \frac{\partial n_-}{\partial t} &= -\Gamma [n_- - n_-^{(\text{eq})}]. \end{aligned} \quad (14)$$

An important feature of magnetic deflagration is the strong temperature dependence of the heat capacity and thermal conductivity at low temperatures. As the temperatures before and behind the deflagration front can differ by an order of magnitude, this effect cannot be neglected. The phonon heat capacity  $C_{\text{ph}}$  has the form

$$C_{\text{ph}} = A k_B \left( \frac{T}{\Theta_D} \right)^\alpha, \quad (15)$$

where  $\alpha=3$  in three dimensions,  $A$  is a numerical factor, and  $\Theta_D$  is the Debye temperature. At low temperatures, only acoustic phonons are excited, whereas high-energy optical phonons are frozen out. Thus, one can use the  $A$  value for the simple model of a crystal,<sup>18</sup>  $A = 12\pi^4/5 \approx 234$ , that is in a good agreement with measurements<sup>13</sup> on  $\text{Mn}_{12}$ . The thermal diffusivity

$$\kappa = k / C_{\text{ph}} \quad (16)$$

depends on the average mean free path of thermal phonons. At low temperatures, the main scattering mechanism is scattering on impurities, so that (see Ref. 19, and references therein)

$$\kappa \propto T^{-\beta}, \quad \beta = 13/3. \quad (17)$$

Accordingly, the thermal conductivity behaves as

$$k \propto T^{-\gamma}, \quad \gamma = \beta - \alpha = 4/3 \quad (18)$$

for  $\alpha=3$ .

The heat-conduction equation can be brought into a more elegant form by choosing the phonon energy  $\mathcal{E}$  as the dynamical variable. Using  $C_{\text{ph}} = d\mathcal{E}/dT$ , one obtains

$$\frac{\partial \mathcal{E}}{\partial t} = \nabla \cdot \kappa \nabla \mathcal{E} - \Delta E \frac{\partial n_-}{\partial t}. \quad (19)$$

This form of the equations is convenient for the study of the stationary deflagration front as it allows one to immediately obtain the first integral of the heat-conduction equation.

Alternatively, one can use

$$K = \int_{T_0}^T k(T') dT' \quad (20)$$

as the temperature variable, with  $T_0$  being a reference temperature. With this choice, the first expression in Eqs. (14) takes the form

$$\frac{1}{\kappa} \frac{\partial K}{\partial t} = \nabla^2 K - \Delta E \frac{\partial n_-}{\partial t}, \quad (21)$$

while in the second equation, one should use  $T = T(K)$  in the expression for  $\Gamma$ . This form of equations is convenient for the study of the deflagration threshold in the case when the temperature along the boundary of the crystal varies.

### III. THERMAL RUNAWAY AND ITS THRESHOLD

Deflagration begins with a thermal runaway in a part of the sample that has a lower barrier  $U$  or a higher temperature  $T$  than the surrounding area. Thermal runaway needs some time to develop. We call it the ignition time  $\tau_{\text{ig}}$ . The shortest ignition time is achieved if the heat released by the relaxation remains in the sample and does not escape through its boundaries. We denote this ignition time  $\tau_{\text{ig}}^{(\infty)}$ , as it is related to the ignition in the infinite sample, see below. If the rate of heat transfer out of the sample is sufficiently high, the igni-

tion does not occur. This explains why small crystals do not exhibit magnetic avalanches. In this section, we obtain the expression for the ignition rate  $\Gamma_{\text{ig}}^{(\infty)} \equiv 1/\tau_{\text{ig}}^{(\infty)}$  and find the dimensionless parameter  $\delta$  that defines the threshold of thermal runaway, or the ignition of deflagration. Also, we will find the parameter that justifies the validity of the explosive approximation  $n_- \Rightarrow n_{-,i}$  ( $n_{-,i}$  is the initial value of  $n_-$ ) that will be used below.

Consider a sample in a thermal contact with the environment. The temperature of the environment can change along the interface with the sample, and the main role in the ignition plays its maximal value that we call  $T_0$ . In Eqs. (14), it is convenient to switch to the reduced variables

$$\theta \equiv W_0 \frac{T - T_0}{T_0}, \quad \tilde{n} \equiv \frac{n_-}{n_{-,i}}, \quad (22)$$

where  $W_0$  is defined by Eq. (9) with  $T=T_0$  and  $n_{-,i}$  is the initial value of the metastable population. Linearization of the argument of  $\Gamma(T)$  on  $\theta$  leads to the system of equations

$$\frac{\partial \theta}{\partial \tau} = \frac{1}{2\delta} \nabla_x^2 \theta + e^{\theta} \tilde{n}, \quad \nu_0 \frac{\partial \tilde{n}}{\partial \tau} = -e^{\theta} \tilde{n}, \quad (23)$$

where  $\tau \equiv \Gamma_{\text{ig}}^{(\infty)} t$  is the reduced time. The reduced space variable  $x$  is normalized by  $R$ , the latter being the minimal distance from the center of the sample to its boundaries. (For a 1d sample of length  $L$ , one has  $R=L/2$ , whereas for cylindrical and spherical samples  $R$  is the radius.) The ignition rate  $\Gamma_{\text{ig}}^{(\infty)}$  is given by

$$\Gamma_{\text{ig}}^{(\infty)} = \nu_0 \Gamma(T_0), \quad (24)$$

where

$$\nu_0 \equiv \frac{U}{k_B T_0} \frac{n_{-,i} \Delta E}{k_B T_0} \frac{1}{C_{\text{ph},0}/k_B} \quad (25)$$

and  $C_{\text{ph},0}$  is the phonon heat capacity at  $T=T_0$ . In the second of Eqs. (23), we assumed full burning,  $n_-^{(\text{eq})} \Rightarrow 0$ . The validity condition for this will be obtained below. The parameter  $\delta$  in the first of Eqs. (23) can be cast in different forms as

$$\delta \equiv \frac{\Gamma_{\text{ig}}^{(\infty)}}{\Gamma_{\kappa}} = \left( \frac{R}{l_0} \right)^2 = \frac{U}{k_B T_0} \frac{n_{-,i} \Delta E}{k_B T_0} \frac{R^2 \Gamma(T_0)}{2k_0/k_B}, \quad (26)$$

where  $k_0$  is thermal conductivity  $k$  at  $T=T_0$ ,

$$\Gamma_{\kappa} = 2\kappa_0/R^2 \quad (27)$$

is the rate of thermal equilibration within the sample at  $T=T_0$ , and  $\kappa_0$  is the thermal diffusivity  $\kappa$  at  $T=T_0$ . In Eq. (26),  $l_0$  is the characteristic thermal length,

$$l_0 = \sqrt{2\kappa_0/\Gamma_{\text{ig}}^{(\infty)}}, \quad (28)$$

also at  $T=T_0$ .

Note that in cases of practical interest,  $\nu_0$  of Eq. (25) is a large parameter since it is a product of three large parameters at low temperatures. Since  $\nu_0 \gg 1$ , the evolution of  $\tilde{n}$  is much slower than that of  $\theta$ , so that one can approximately replace  $\tilde{n} \Rightarrow 1$  to obtain an isolated equation for  $\theta$ . This is what we call the explosive approximation or the explosive limit. (Indeed, for explosives, the parameter  $\nu_0$  is very large, so that

the problem of their stability can be considered without taking into account that a small part of the explosive has already burned and the heat release has been reduced because of this.)

Let us consider now the thermal runaway in an infinite or thermally isolated sample dropping the diffusion term in the first of Eqs. (23). Within the explosive approximation, one obtains the isolated equation  $\partial \theta / \partial \tau = e^{\theta}$  that has the solution  $\theta(\tau) = -\ln(1-\tau)$ , reaching infinity exactly at  $\tau=1$ . In real units, it corresponds to  $t = \tau_{\text{ig}}^{(\infty)}$ . Of course, as the ignition occurs, the deviation of  $T$  from  $T_0$  becomes large; thus, the linearized term  $e^{\theta}$  and the replacement  $\tilde{n} \Rightarrow 1$  become invalid. Nevertheless, the dominant contribution into the ignition time comes from the time range  $\theta \sim 1$ , where still  $T - T_0 \ll T_0$  and the equation  $\partial_t \theta = e^{\theta}$  is valid.

The low-temperature explosive approximation  $\tilde{n} \Rightarrow 1$  introduced above drastically simplifies the problem of the ignition of deflagration and allows one to understand it in simple terms. With  $\tilde{n}=1$ , the temperature of the sample is the only relevant variable, and its dynamics is determined by the competition of the two terms. One of them is the heat release due to the relaxation that is strongly nonlinear in temperature. The other one is the heat loss due to the heat conduction that is linear on temperature but contains spatial derivatives. There are two scenarios if one starts with the sample having a uniform temperature  $T=T_0$  that coincides with the constant temperature of the sample boundaries. In the first scenario, the temperature increases because of the heat release, typically with a maximum at the center of the sample, until a sufficient temperature gradient develops that provides the balance between the heat release and heat loss through the boundaries. The resulting state is the stationary state of the system. In the second scenario, the heat loss through the boundaries is insufficient to balance the increase of the heat release due to the rise of temperature. This happens, in particular, if the sample is sufficiently large. In this case, there is no stationary state, and the temperature growth, slow at the beginning, leads to a thermal runaway. Changing one of the parameters (sample size, energy barrier, temperature at the boundaries, and initial magnetization), one can reach the situation in which the stationary state disappears and the runaway begins. We call it the ignition threshold.

In Sec. IV, we present analytical and numerical results for the ignition threshold in different cases in the explosive limit. We will see that the ignition is mainly controlled by the parameter  $\delta$  of Eq. (26). In particular, in the simplest case of the uniform energy barrier and constant temperature  $T_0$  maintained at the boundaries (uniform conditions), the ignition threshold corresponds to  $\delta = \delta_c \sim 1$ . The exact value  $\delta_c$  depends on the geometry of the sample. In particular, in one dimension,  $\delta_c \approx 0.439$ . This allows one to obtain a relation between the temperature  $T_0$  and the barrier  $U$  at the ignition threshold that also depends on the sample size  $R$  and other parameters. In terms of dimensionless parameters

$$\bar{T}_0 \equiv \frac{k_B T_0}{U}, \quad A \equiv \frac{R^2 \Gamma_0 n_{-,i}}{2k(\bar{T}_0)/k_B} \quad (29)$$

[see Eqs. (3) and (12)], one can write Eq. (26) in the form

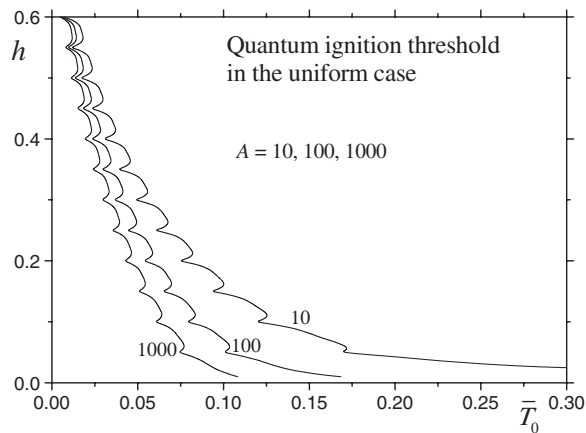


FIG. 2. The dependence of the magnetic field that ignites deflagration on the temperature of the crystal of  $\text{Mn}_{12}$ . Dimensionless parameters are given by Eqs. (3) and (29).

$$\delta = A \frac{4hu(h)}{\bar{T}_0^2} \exp\left[-\frac{u(h)}{\bar{T}_0}\right], \quad (30)$$

where  $u(h)$  is given by  $u(h)=(1-h)^2$  for the classical model and by Eq. (8) with account of spin tunneling. Resolving the threshold equation  $\delta=\delta_c$  requires the knowledge of the temperature dependence of thermal conductivity  $k$ . It turns out (see below), however, that the exact form of  $k(\bar{T}_0)$  given by Eq. (18) is not essential. The results for  $k(T)=\text{const}$  and thus  $A=\text{const}$  are shown in Fig. 2 for three different values of  $A$ . One can see that increasing  $A$  (say, due to the increasing of the sample size  $R$ ) leads to the decrease of the critical values of  $\bar{T}_0$  and  $h$ . In the realistic case of the large Arrhenius exponent in Eq. (30), the dependence on  $A$  and thus on  $k$  is logarithmic.

#### IV. IGNITION THRESHOLD IN MOLECULAR MAGNETS

In this section, we work out the ignition threshold in different cases. At first, in the uniform case, the exact values of  $\delta_c \sim 1$  will be obtained in one, two, and three dimensions. Here, the ignition occurs in a large region around the center of the sample. Then, the nonuniform cases in which the barrier  $U$  changes in space or the environment temperature is different at different ends of the sample will be considered. In the nonuniform cases, ignition occurs in a narrow region where the conditions for this are most favorable. Then, the heat flow out of this region to the rest of the sample makes ignition more difficult, resulting in  $\delta_c \gg 1$ .

##### A. Ignition threshold under uniform conditions

###### 1. Ignition threshold in one dimension

Consider a slab of thickness  $L=2R$ . We will see that at  $W \gg 1$ , if the constant temperature  $T_0$  is maintained at the boundaries of the slab, the solution for  $T$  at the ignition threshold only slightly deviates from  $T_0$ . In this case, one can linearize the problem around  $T_0$  using the temperature devia-

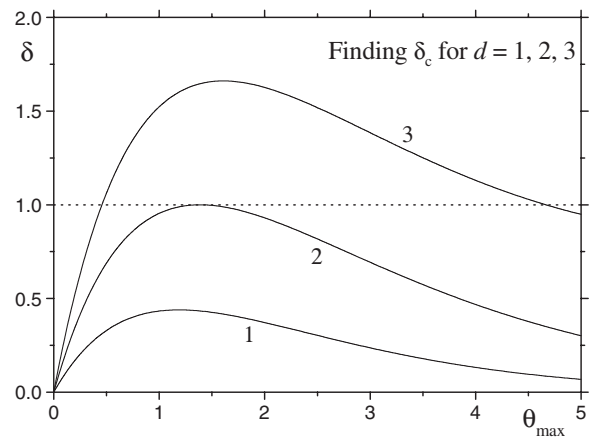


FIG. 3. Plot of  $\delta(\theta_{\max})$  for  $d=1,2,3$  that allows one to obtain the ignition threshold from the maximum of these curves.

tion  $\theta$  of Eq. (22) and set  $k \Rightarrow k_0$ . With  $\partial T/\partial t=0$  in the stationary case, one obtains the equation

$$\frac{d^2\theta}{dx^2} + 2\delta e^\theta = 0, \quad \theta(\pm 1) = 0. \quad (31)$$

The first integral of this equation is

$$\left(\frac{d\theta}{dx}\right)^2 + 4\delta(e^\theta - e^{\theta_{\max}}) = 0, \quad (32)$$

where  $\theta_{\max}$  is the integration constant that equals the maximal value of  $\theta$  achieved in the middle of the sample. Integrating Eq. (32), one obtains

$$\theta(x) = \theta_{\max} - 2 \ln \cosh(\sqrt{\delta e^{\theta_{\max}}} x), \quad (33)$$

where the value of  $\theta_{\max}$  follows from the boundary conditions  $\theta(\pm 1)=0$ . To find the ignition threshold, one can solve this equation for  $\delta$ :

$$\delta = e^{-\theta_{\max}} \ln^2[e^{\theta_{\max}/2} + \sqrt{e^{\theta_{\max}} - 1}]. \quad (34)$$

The dependence  $\delta(\theta_{\max})$  is shown in Fig. 3. It has a maximum at  $\theta_{\max} = \theta_{\max,c} = 1.18684$ . The maximal value of  $\delta$ ,

$$\delta_c = 0.439229, \quad (35)$$

corresponds to the ignition threshold. Indeed, for  $\delta < \delta_c$ , there are two solutions for  $\theta_{\max}$ , and the smaller of the two corresponds to the stationary solution of the heat-conduction equation. For  $\delta > \delta_c$ , the stationary solution disappears.

###### 2. Ignition threshold in two and three dimensions

For a cylindrical ( $d=2$ ) and spherical ( $d=3$ ) samples, the generalization of Eq. (31) is

$$\frac{d^2\theta}{dr^2} + \frac{d-1}{r} \frac{d\theta}{dr} + 2\delta e^\theta = 0, \quad (36)$$

with  $r$  normalized by  $R$  and with the boundary conditions  $\theta'(0)=0$  and  $\theta(1)=0$ . For  $d=2$ , the exact solution of Eq. (36) is

$$\theta(r) = 2 \ln \frac{2}{1 + \sqrt{1 - \delta} + (1 - \sqrt{1 - \delta})r^2}. \quad (37)$$

Its maximal value

$$\theta_{\max} = 2 \ln \frac{2}{1 + \sqrt{1 - \delta}} \quad (38)$$

is achieved at  $r=0$ . The ignition threshold can be found by the same method as in one dimension. Resolving this equation for  $\delta$ , one obtains

$$\delta = 4e^{-\theta_{\max}}(e^{\theta_{\max}/2} - 1). \quad (39)$$

This function has a maximum at  $\theta_{\max} = \theta_{\max,c} = 2 \ln 2 \approx 1.3863$ , and the corresponding critical value of  $\delta$  is

$$\delta_c = 1. \quad (40)$$

For  $d=3$ , we are unable to find the solution of Eq. (36) in terms of known functions. Numerical solution for the ignition threshold in three dimensions consists of the following steps: (i) One solves Eq. (36) with the boundary conditions  $\theta'(0)=0$  and  $\theta(0)=\theta_{\max}$  and  $\delta$  as a free parameter. (ii) One finds  $\delta$  as a function of  $\theta_{\max}$  from the boundary condition  $\theta(1)=0$ . (iii) One finds critical parameters from the maximum of  $\delta(\theta_{\max})$ . Our results for  $d=1,2,3$  are listed below,

$d$	$\delta_c$	$\delta_c/d$	$1/\delta_c$	$\theta_{\max,c}$
1	0.4392	0.4392	2.277	1.187
2	1	0.5	1	1.386
3	1.661	0.5537	0.6020	1.607

(41)

One can see that approximately  $\delta_c \propto d$ . The curves  $\delta(\theta_{\max})$  are plotted in Fig. 3.

### B. Ignition threshold in the presence of field gradient

Consider a one-dimensional problem of ignition with temperature at both ends maintained at  $T_0$  and the barrier  $U$  varying in space due to the gradient of the bias field. Although the relative variation of  $U$  is small, the effect can be large for large Arrhenius factors  $W$  as its variation  $\delta W$  can be large. Assuming that the barrier is the lowest at the left end of the sample and the field gradient is small and constant, one can write

$$\delta W \cong w(1+x) - \theta. \quad (42)$$

The equation for the stationary temperature profile becomes

$$\frac{d^2 \theta}{dx^2} + 2\delta e^{-w(1+x)+\theta} = 0, \quad \theta(\pm 1) = 0. \quad (43)$$

For  $w \sim 1$ , Eq. (31) can only be solved numerically. Here, instead of plotting  $\delta$  vs  $\theta_{\max}$ , it is more convenient to plot  $\delta$  vs  $\theta'(-1)$ . Numerical results for temperature profile  $\theta(x)$  and heat-release profile  $q(x) \propto \exp[-w(1+x)+\theta]$  at the ignition threshold are shown in Fig. 4. As the field gradient goes up, the maxima of these curves shift toward the end of the

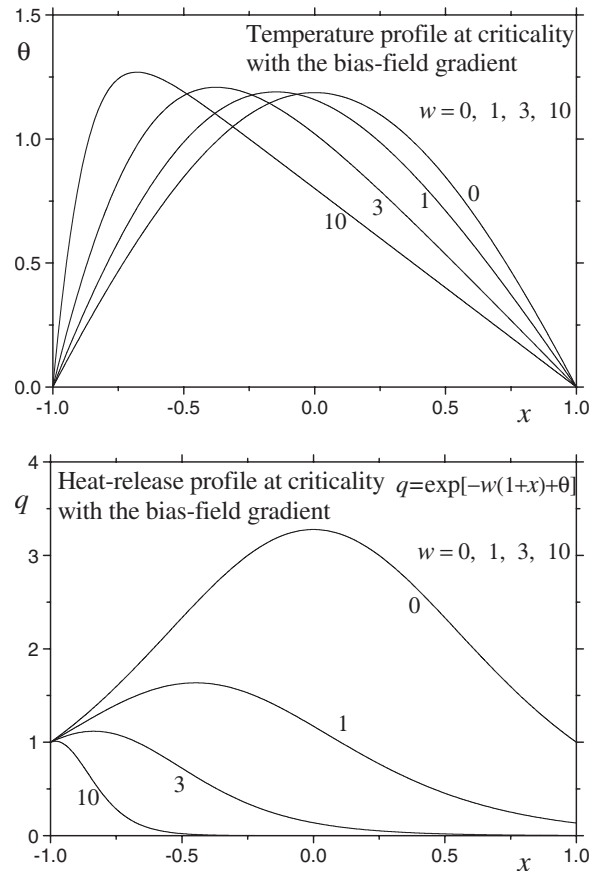


FIG. 4. Numerical results for temperature and heat-release profiles at the ignition threshold,  $\delta = \delta_c$ , in the model with bias-field gradient.

sample where the barrier is lower. The threshold condition  $\delta_c(w)$  is shown in Fig. 5. The value of  $\delta_c$  increases with  $w$ , since the favorable condition for burning is realized in a more and more narrow region at the left end of the sample, and there is an increasing heat flow out of this region in both directions.

In the case of  $w \gg 1$ , the ignition occurs very close to the left end,  $x = -1$ , and the heat release proportional to

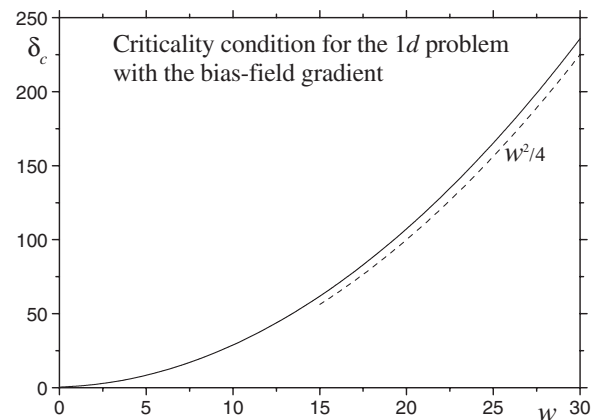


FIG. 5. Dependence of the ignition threshold on the bias-field gradient, see Eq. (49).

$\exp[-w(1+x)+\theta]$  is very close to zero except in the vicinity of the left end. The temperature profile for  $w \gg 1$  consists of two regions: Very close to the left end, the temperature rises sharply to the maximal temperature  $\theta_{\max}$  and then goes linearly down to zero at the right end. Thus, for  $w \gg 1$ , one can introduce a new variable  $u \equiv w(1+x)$  and a new function  $\vartheta = \theta - u$  and replace Eq. (43) by

$$\frac{d^2\vartheta}{du^2} + 2\tilde{\delta}e^{\vartheta} = 0, \quad \tilde{\delta} \equiv \frac{\delta}{w^2}, \quad (44)$$

with the boundary conditions  $\vartheta(0)=0$  and  $\vartheta'(\infty)=-1$ . This equation is similar to Eq. (31) and its solution reads

$$\vartheta(u) = \vartheta_{\max} - \ln \cosh^2(\sqrt{\tilde{\delta}e^{\vartheta_{\max}}}(u - u_{\max})), \quad (45)$$

where  $\vartheta_{\max}$  and  $u_{\max}$  are integration constants. From the boundary condition  $\vartheta'(\infty)=-1$ , one obtains  $2\sqrt{\tilde{\delta}e^{\vartheta_{\max}}}=1$  and thus

$$\vartheta_{\max} = \ln \frac{1}{4\tilde{\delta}}. \quad (46)$$

Then, the other boundary condition,  $\vartheta(0)=0$ , gives

$$u_{\max} = 2 \operatorname{arccosh} \frac{1}{2\sqrt{\tilde{\delta}}}. \quad (47)$$

Since  $\vartheta_{\max} \geq 0$ , the ignition threshold is defined by

$$\tilde{\delta}_c = \frac{1}{4}, \quad \delta_c = \frac{w^2}{4}. \quad (48)$$

For  $\delta = \delta_c$ , one has  $u_{\max}=0$ , that is, the ignition occurs at the left boundary. Corrections to Eq. (44) move the maximal-temperature point a little away from the edge of the sample. Comparing this situation with the uniform case with the same barrier at the left end (the minimal barrier), one can see that in the case of  $w \gg 1$ , the ignition requires a much higher temperature  $T_0$ .

The constant  $w$  in Eq. (42) can be expressed via the gradient of the bias field with the help of Eq. (5):

$$w = \frac{dW}{dx} = W_0(1-h)|\Delta h|, \quad (49)$$

where  $\Delta h$  is the change of  $h$  across the sample. In terms of the energy bias  $\Delta E$  defined by Eq. (6), one has

$$w = \frac{1-h}{4} \frac{\Delta(\Delta E)}{k_B T_0}, \quad (50)$$

where  $\Delta(\Delta E)$  is the change of the energy bias across the sample. Note that at a very low temperature  $T_0$ , the condition  $w \gg 1$  does not necessarily require a large field gradient. Because of the field gradient, the Arrhenius factor  $W$  increases by 1 at the characteristic distance

$$l_H \equiv \frac{2R}{w} = \frac{L}{w} = \frac{L}{W_0(1-h)|\Delta h|} \quad (51)$$

from the end. It is the width of the ignition region near the low-barrier end. In the case of  $w \gg 1$ , that is  $l_H \ll L$ , the far

end with the highest barrier becomes irrelevant for the ignition, and the ignition threshold  $\delta = \delta_c$  that follows from Eqs. (26) and (48) becomes

$$l_H = l_0. \quad (52)$$

For a cylinder of radius  $R$  with the bias field linearly changing along its symmetry axis, this condition holds if  $l_H \ll R$ , so that the heat flows along the cylinder axis  $z$  away from the face with the lowest barrier rather than toward the side walls of the cylinder. The problem then becomes one dimensional.

### C. Ignition threshold in the presence of temperature gradient

While it is experimentally difficult to create a large gradient of the bias field over the length of a small crystal, it is relatively easy to break the symmetry of the system by creating a large temperature gradient. This can be done by, e.g., maintaining temperature  $T_0$  at the left end and having  $T_1 < T_0$  at the right end of a  $1d$  sample. If these two temperatures differ essentially, one has to take into account the temperature dependence of thermal conductivity  $k(T)$  that is strong at low  $T$ , see Eq. (18). In this case, it is more convenient to use  $K$  defined by Eq. (20) instead of  $T$ . As the ignition occurs closer to the hot left end, it is convenient to choose  $T_0$  as the reference temperature and introduce

$$\theta \equiv W_0 \frac{K}{k_0 T_0} \quad (53)$$

that generalizes Eq. (22), with  $k_0 \equiv k(T_0)$ . The relaxation rate can be expanded similarly to the above,

$$\Gamma(T(K)) \cong \Gamma(T_0) \exp\left(W_0 \frac{\delta T}{T_0}\right) \cong \Gamma(T_0) e^{\theta}. \quad (54)$$

The applicability of this expansion requires  $|\delta T|/T_0 \ll 1$ . However, in the case of  $W_0 \gg 1$ , this expansion practically works in the whole range of  $\delta T < 0$ , since the burning rate  $\Gamma$  becomes negligibly small long before the condition  $|\delta T|/T_0 \ll 1$  is violated. In the stationary state,  $\theta(x)$  satisfies the same Eq. (31) but with the boundary conditions

$$\theta(-1) = 0, \quad \theta(1) \equiv \theta_1 = W_0 \frac{K(T_1)}{k_0 T_0} \leq 0. \quad (55)$$

In the absence of the heat release due to burning, the solution for  $\theta$  would be a linear function,  $\theta(x) = (1+x)\theta_1/2$ . An estimate for the width  $l_T$  of the region near the hot end where the ignition occurs can be obtained by setting  $\theta(x) \sim -1$ . In real units, ignition occurs at the distance of order

$$l_T = 4R/|\theta_1|, \quad (56)$$

where the numerical factor of 4 anticipates Eq. (62). For the very cold right end,  $|\theta_1| \gg 1$ , one has  $l_T \ll R$ . The first integral of Eq. (31) is Eq. (32) in which the maximum  $\theta = \theta_{\max}$  can be achieved at some  $x_{\max}$  shifted from the central point  $x=0$ . The solution for  $\theta(x)$  reads

$$\theta(x) = \theta_{\max} - 2 \ln \cosh[\sqrt{\delta} e^{\theta_{\max}}(x - x_{\max})], \quad (57)$$

which is the generalization Eq. (33). Elimination of  $x_{\max}$  using the boundary conditions and solving for  $\delta$  yield

$$\delta = \frac{1}{4} e^{-\theta_{\max}} \ln^2[(e^{\theta_{\max}/2} + \sqrt{e^{\theta_{\max}} - 1}) \times (e^{(\theta_{\max} - \theta_1)/2} + \sqrt{e^{\theta_{\max} - \theta_1} - 1})], \quad (58)$$

cf. Eq. (34). Computing the maximum of this function on  $\theta_{\max}$  allows us to determine  $\delta_c$  for any value of  $\theta_1$ .

If the temperature at the right end is low,  $-\theta_1$  is a large positive value, so that Eq. (58) is simplified. In this case, at the ignition threshold, one has  $\theta_{\max} \ll 1$ , so that Eq. (58) becomes

$$\delta \cong \frac{\theta_1^2}{16} e^{-\theta_{\max}} \left( 1 + \frac{4 \ln 2}{|\theta_1|} + \frac{4\sqrt{\theta_{\max}}}{|\theta_1|} \right). \quad (59)$$

The maximum of the right-hand side is attained at  $\theta_{\max} = \theta_{\max,c} \cong 4/\theta_1^2 \ll 1$ . Thus, the ignition threshold is defined by

$$\delta_c \cong \left( \frac{|\theta_1| + 2 \ln 2}{4} \right)^2 + \frac{1}{4} \cong \left( \frac{W_0 K(T_1)}{4 k_0 T_0} \right)^2. \quad (60)$$

The maximal-temperature point at the ignition threshold is

$$x_{\max,c} \cong -1 + 8/\theta_1^2, \quad (61)$$

which is close to the left end. One can see that for  $|\theta_1| \gg 1$ , the value of  $\delta_c$  is large, so that much larger  $L$  is needed to reach the threshold for the same temperature  $T_0$ , as compared to the uniform case. The ignition threshold  $\delta = \delta_c$  is equivalent to

$$l_T = l_0, \quad (62)$$

where  $l_T$  is given by Eq. (56). This result is similar to Eq. (52). The numerically obtained dependences  $\delta_c(|\theta_1|)$  and  $x_{\max,c}(|\theta_1|)$  are shown in Fig. 6.

The remaining task is to relate the temperature-bias parameter  $\theta_1$  to the temperatures at the ends,  $T_0$  and  $T_1$ . At a constant thermal conductivity  $k$ , one obtains

$$\theta_1 = -W_0 \left( 1 - \frac{T_1}{T_0} \right) \quad (63)$$

that tends to  $-W_0$  in the limit  $T_1 \rightarrow 0$ . Since  $W_0 \gg 1$ , there is a strong suppression of the ignition by the cold end. The effect is even stronger for the power-law dependence of  $k$  given by Eq. (18). Parametrization

$$k(T) = k_0 \left( \frac{T}{T_0} \right)^{-\gamma} \quad (64)$$

and integration in Eq. (20), with the lower limit being  $T_0$ , yields

$$K(T) = -\frac{k_0 T_0}{\gamma - 1} \left[ \left( \frac{T_0}{T} \right)^{\gamma-1} - 1 \right]. \quad (65)$$

Now, one obtains

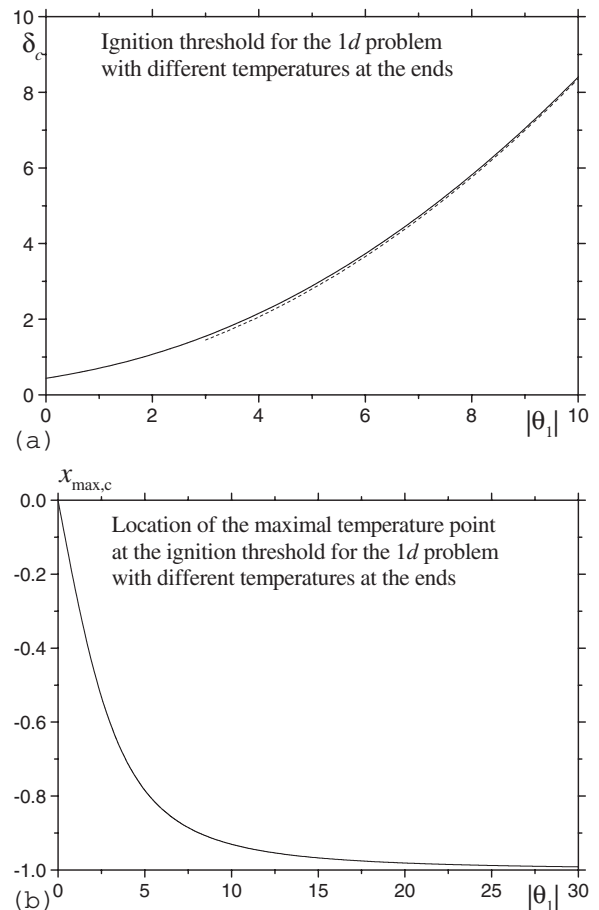


FIG. 6. Numerical results for (a)  $\delta_c$  and (b)  $x_{\max,c}$  vs the temperature-bias parameter  $\theta_1$  for the 1d model with different temperatures at the ends.  $x=0$  corresponds to the center of the sample. The dashed line in (a) is the asymptote  $\delta_c \cong (|\theta_1| + 2 \ln 2)^2 / 16 + 1/4$  at  $|\theta_1| \gg 1$ .

$$\theta_1 = -\frac{W_0}{\gamma - 1} \left[ \left( \frac{T_0}{T_1} \right)^{\gamma-1} - 1 \right], \quad (66)$$

and for  $|\theta_1| \gg 1$ ,

$$\delta_c \cong \left\{ \frac{W_0}{4(\gamma - 1)} \left[ \left( \frac{T_0}{T_1} \right)^{\gamma-1} - 1 \right] \right\}^2. \quad (67)$$

In the realistic case given by Eq. (18), one has  $\gamma - 1 = 1/3$ . That is, if  $T_1$  goes to zero,  $\theta_1$  becomes infinite negative and  $\delta_c$  diverges. This means that for a sample of any size, one can suppress the ignition by making the temperature of the cold end very close to zero. This is a consequence of the divergence of thermal conductivity at  $T=0$ .

## V. RATE OF IGNITION OF DEFLAGRATION IN MOLECULAR MAGNETS

Above the ignition threshold,  $\delta > \delta_c$ , the heat loss via heat conduction cannot compensate the heat release due to burning, and there is no stationary solution for the temperature. The temperature growth leads to a thermal runaway after the ignition time  $\tau_{ig}$ , followed by the deflagration. At first, we

investigate the ignition time within the explosive approximation,  $n_- \Rightarrow n_{-,i}$ , in terms of  $\theta$  defined by Eq. (22) or (53). Then, we study deviations from the explosive approximation using a more general system of equations containing both  $\theta$  and  $n_-$ . The initial condition in all examples considered in this section is the thermal equilibrium reached in the absence of relaxation, for instance, a uniform temperature throughout the sample. This is the most transparent case theoretically, but it may be difficult to realize in experiment if the ignition rate is large. At the end of this section, we discuss other kinds of initial conditions.

### A. Explosive approximation

At low temperatures, the explosive approximation is valid, see Sec. III, and one can use the autonomous heat-conduction equation in terms of  $\theta$ . In particular, for the 1d model with the uniform energy barrier, this equation has the form

$$\frac{\partial \theta}{\partial \tau} = \frac{1}{2\delta} \frac{\partial^2 \theta}{\partial x^2} + e^\theta, \quad (68)$$

where  $\tau$ ,  $x$ , and  $\delta$  are defined by Eqs. (23), (31), and (26), respectively. Strictly speaking, there is a factor  $\kappa_0/\kappa(\theta)$  in the left-hand side of this equation, where  $\kappa_0$  corresponds to  $T=T_0$  ( $\theta=0$ ). However, this factor is very close to 1 in the region where ignition occurs. During the ignition time,  $\theta$  formally reaches infinity at some  $x=x_{ig}$ . It is difficult to solve Eq. (68) analytically. Clearly, for a uniform, infinite or thermally insulated sample,  $\delta \rightarrow \infty$ , one should obtain the ignition rate  $\Gamma_{ig}^{(\infty)}$  of Eq. (24). An insight into the dependence of  $\Gamma_{ig}$  on the coupling to the environment can be gained if in the diffusive term one makes the replacement  $\Delta\theta \Rightarrow -(2d/R^2)\theta$ . In the 1d case, this amounts to  $\partial^2\theta/\partial x^2 \Rightarrow -2\theta$  in Eq. (68). Then, the simplified equation can be integrated and yields the ignition rate

$$\Gamma_{ig} = \frac{\Gamma_{ig}^{(\infty)}}{\int_0^\infty \frac{d\theta}{e^\theta - \theta/\delta}} \cong \Gamma_{ig}^{(\infty)} \begin{cases} 1 - \frac{1}{4\delta}, & \frac{1}{\delta} \ll 1 \\ \frac{\sqrt{2e(e-1/\delta)}}{2\pi}, & e - \frac{1}{\delta} \ll 1. \end{cases} \quad (69)$$

Above the ignition threshold,  $\delta > \delta_c = e^{-1}$ ,  $\Gamma_{ig}$  decreases with decreasing  $\delta$  and turns to zero with a square-root singularity at  $\delta_c$ . The value of  $\delta_c$  in this approximation is reasonably close to the exact value given by Eq. (35), and the whole dependence  $\Gamma_{ig}(\delta)$  does not deviate much from the accurate numerical solution of Eq. (68) in the uniform case.

To solve Eq. (68) numerically, one should avoid the divergence of  $\theta$  by changing to another variable, e.g.,  $p = e^{-\theta}$ . The ignition can be detected from  $p$  turning zero at some  $x$  that we call the *ignition point*,  $x=x_{ig}$ . Figure 7 shows the dependence  $\Gamma_{ig}(\delta)$  obtained numerically in the case of different temperatures at the two ends (see Sec. IV C). The initial condition was  $\theta(x)$  changing linearly between zero and  $\theta_1$ . In the uniform case,  $\theta_1=0$ , the solution behaves qualitatively similar to the approximate solution given by Eq. (69), except

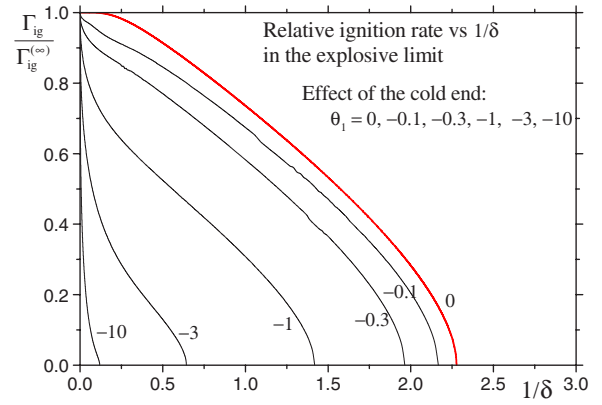


FIG. 7. (Color online) Ignition rate  $\Gamma_{ig}$  vs  $1/\delta$  in the 1d model with different temperatures at the ends. Parameter  $\theta_1$  is given by Eq. (22).

for small values of  $1/\delta$ . The ignition rate has a square-root singularity at  $\delta = \delta_c$ . For  $\delta < \delta_c$ , the variable  $p$  does not turn zero at any point for any time; thus, the ignition rate is zero. Lowering the temperature of the cold end leads to the decrease of  $\Gamma_{ig}$  and the increase of  $\delta_c$ . Note a striking singularity in the large-size limit  $\delta \gg 1$  in the presence of the temperature bias.

### B. Beyond the explosive approximation

Let us check now how practically good is the explosive approximation  $\tilde{n} \Rightarrow 1$  for  $\nu_0 \gg 1$  by solving the full system of equations [Eq. (23)] in one dimension. Numerical solution of these equations shows that the ignition rate decreases (also for the infinite sample) and the value of  $\delta_c$  increases as the result of the relaxation of  $\tilde{n}$  controlled by  $\nu_0$ . An interesting effect is the change of the critical behavior of  $\Gamma_{ig}$  at the ignition threshold for any finite  $\nu_0$ . As we have seen above,  $\tau_{ig}$  that follows from Eq. (68) becomes very long near the threshold. During such a long time, there will be a considerable relaxation of  $\tilde{n}$  even for large  $\nu_0$ . As a result, the critical behavior of  $\Gamma_{ig}$  changes, and for any finite  $\nu_0$ , there is a jump of  $\Gamma_{ig}$  at the threshold, see Fig. 8. Even for  $\nu_0=100$ , the

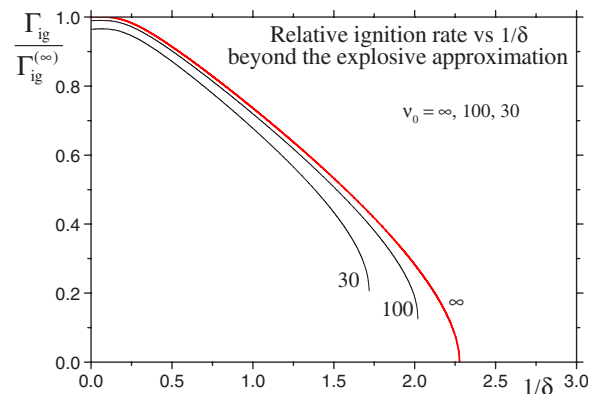


FIG. 8. (Color online) Ignition rate  $\Gamma_{ig}$  vs  $1/\delta$  in the 1d model beyond the explosive approximation with equal temperatures at the ends.

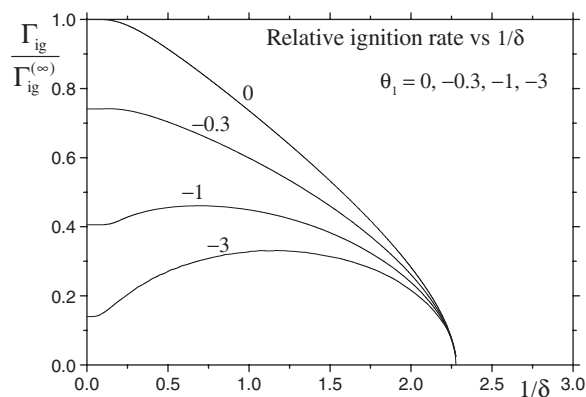


FIG. 9. Ignition rate  $\Gamma_{\text{ig}}$  vs  $1/\delta$  in the  $1d$  model with uniform initial condition  $\theta = \theta_1 < 0$  followed by a rapid temperature rise to  $\theta = 0$  at the ends of the sample.

results for  $\Gamma_{\text{ig}}$  differ strongly from those obtained within the explosive approximation.

All results for the ignition rate can also be numerically obtained from the solution of the initial system of equations, Eqs. (14). In this case, the moment of ignition is identified by the highest time derivatives of  $T$  or  $\tilde{n}$ .

Beyond the explosive approximation, the ignition scenarios differ slightly from those described above. Above the ignition threshold, thermal runaway occurs in spite of the depletion of  $n_-$  caused by its relaxation. Below the ignition threshold, the temperature increases, reaches a maximum, and then slowly decreases because of the slow relaxation of  $\tilde{n}$ . There is no stationary solution but a bifurcation between the two types of the behavior of  $T(t)$ .

### C. Fast temperature rise at the boundaries

The initial condition in a form of a stationary temperature profile in the absence of relaxation could be, in principle, achieved by the rapid change of the bias field so that the barrier is decreased and ignition process can start. In this case, the magnetic field should change much faster than the development of ignition. This may be difficult to achieve because of a large time constant of electromagnets producing strong magnetic fields. It would be much easier to rapidly increase the temperature on the surface of the crystal up to  $T_0$ , whereas the initial temperature was  $T_1 < T_0$ . The process is described by Eq. (68) with the initial condition  $\theta(0) = \theta_1 \leq 0$ , where  $\theta_1$  is given by Eq. (22) or (53). The boundary condition at the two ends is a function of time describing a rapid rise from  $\theta = \theta_1$  to  $\theta = 0$ . Note that for  $\theta_1 = 0$ , one recovers the case of the uniform initial temperature considered above. The solution of Eq. (68) depends on two dimensionless parameters,  $\delta$  and  $\theta_1$ .

In the case  $\theta_1 < 0$ , below the ignition threshold, the stationary state studied in Sec. IV is reached asymptotically. Above the ignition threshold, the thermal equilibration rate  $\Gamma_\kappa$  of Eq. (27) becomes smaller than the infinite-sample ignition rate  $\Gamma_{\text{ig}}^{(\infty)}$ ; thus, the process of heat penetration into the sample prior to the ignition becomes crucial. Figure 9 shows the nonmonotonic dependence of the ignition rate on  $1/\delta$

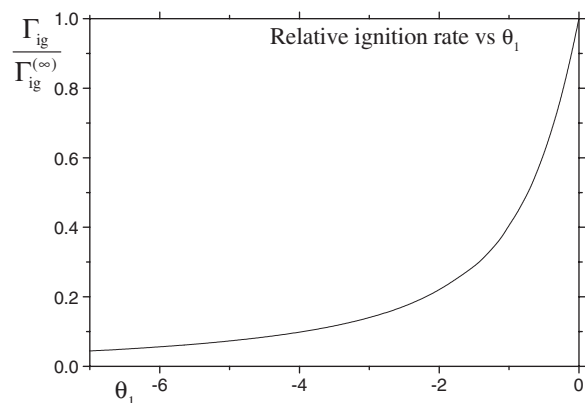


FIG. 10. Ignition rate  $\Gamma_{\text{ig}}$  vs  $\theta_1$  in the semi-infinite  $1d$  model, obtained numerically from Eq. (70).

with a fixed large negative  $\theta_1$ . Note that, since both  $\delta$  and  $\theta_1$  depend on temperature and magnetic field, the dependence of  $\Gamma_{\text{ig}}$  on these variables is different from that shown in Fig. 9. This figure actually shows the size dependence of the ignition rate through  $\delta \propto R^2$ . When the size  $R$  increases above its threshold value, the ignition rate initially grows starting from zero at  $\delta = \delta_c$ . Then, the growth of  $\Gamma_{\text{ig}}$  becomes slower than in the case of the uniform initial temperature,  $\theta_1 = 0$ , since additional time is needed for penetration of the heat into the middle of the sample where ignition occurs. This explains the maxima of the curves in Fig. 9 and the decrease of  $\Gamma_{\text{ig}}$  with increasing size.

Above some value of  $\delta$  that depends on  $\theta_1$ , the ignition point  $x_{\text{ig}}$  splits into two symmetric points away from the center. Far into the instability region, these ignition points move close to the ends and the deflagration front propagates from the ends to the center. In this case, the size of the crystal  $L = 2R$  and the parameter  $\delta$  of Eq. (26) become irrelevant for the ignition, so that one can consider a semi-infinite problem and normalize the distance from the surface by  $l_0$  of Eq. (28) instead of normalizing it by  $R$ . Thus instead of Eq. (68), one obtains

$$\frac{\partial \theta}{\partial \tau} = \frac{1}{2} \frac{\partial^2 \theta}{\partial \tilde{x}^2} + e^\theta. \quad (70)$$

The solution of this equation depends on the single parameter  $\theta_1$ . Figure 10 shows that the ignition rate of a semi-infinite sample decreases with  $|\theta_1|$ , which can also be seen from Fig. 9. Strong suppression of the ignition rate is due to the heat transfer to the cold parts of the sample, which is more important than the heat loss through the surface, the effect we have seen above.

## VI. STRUCTURE AND VELOCITY OF THE DEFLAGRATION FRONT

### A. Thermodynamics of magnetic deflagration

Ignition of deflagration leads to a strong increase of the temperature and relaxation rate that results in equilibration of energy between spin and phonon subsystems. Since deflagration is a fast process, one can use energy conservation, ne-

glecting excited states and the heat loss through the boundaries during deflagration,

$$\mathcal{E}_i + n_{-,i}\Delta E = \mathcal{E}_f + n_-^{(\text{eq})}(T_f)\Delta E. \quad (71)$$

Here,  $\mathcal{E}_{i,f} \equiv \mathcal{E}(T_{i,f})$  are the phonon energies at the initial and final temperatures,  $T_i$  (before the deflagration front) and  $T_f$  (behind the front), respectively,  $n_{-,i}$  is the initial population of the metastable well, and  $n_-^{(\text{eq})}(T_f)$  is the equilibrium value of  $n_-$  at  $T_f$  given by Eq. (11). We will call  $T_f$  the *flame temperature*. Equation (71) is a transcendental equation for the flame temperature  $T_f$ . Since  $T_f \gg T_i$ , the initial phonon energy  $\mathcal{E}_i$  can be neglected.  $T_f$  can be found analytically if  $\mathcal{E}$  has the form

$$\mathcal{E} = \frac{Ak_B\Theta_D}{\alpha+1} \left( \frac{T}{\Theta_D} \right)^{\alpha+1} \quad (72)$$

that follows from Eq. (15) if  $n_-^{(\text{eq})}(T_f)$  is negligibly small—the full-burning case. In this case, from  $\mathcal{E}(T_f) = n_{-,i}\Delta E$ , one obtains

$$T_f = \Theta_D \left( \frac{(\alpha+1)n_{-,i}\Delta E}{Ak_B\Theta_D} \right)^{1/(\alpha+1)}. \quad (73)$$

The full-burning condition is  $k_B T_f \ll \Delta E$ . Using Eq. (6), one can rewrite it in the form of the strong-bias condition

$$h \gg h_{\text{fb}} n_{-,i}^{1/\alpha}, \quad (74)$$

where the full-burning field

$$h_{\text{fb}} \equiv \frac{k_B\Theta_D}{4U_0} \left( \frac{\alpha+1}{A} \right)^{1/\alpha} \quad (75)$$

is a material parameter. With  $\alpha=3$ ,  $A \approx 234$ ,  $U_0 \approx 65$  K, and  $\Theta_D = 38$  K for  $\text{Mn}_{12}$ , one obtains

$$h_{\text{fb}} \approx 0.038. \quad (76)$$

We will see that the speed of the deflagration front is mainly determined by the flame's Arrhenius exponent

$$W_f \equiv \frac{U}{k_B T_f} \quad (77)$$

that can be large if the energy bias  $\Delta E$  is small, resulting in low  $T_f$ . One can express  $W_f$  in the form

$$W_f = \frac{1}{4} \frac{(1-h)^2}{(n_{-,i}h)^{1/(\alpha+1)}} \frac{1}{h_{\text{fb}}^{\alpha/(\alpha+1)}}. \quad (78)$$

The maximal value of  $W_f$  compatible with the full-burning condition (for  $n_{-,i}=1$ ) is given by

$$W_{f,\text{max}} = \frac{(1-h_{\text{fb}})^2}{4h_{\text{fb}}} \approx 6, \quad (79)$$

where the numerical value corresponds to  $\text{Mn}_{12}$  and uses Eq. (76). If  $W_f$  exceeds this value, one cannot neglect  $n_-^{(\text{eq})}(T_f)$  in determining the flame temperature.

## B. Deflagration front

The deflagration is described by the solution of Eqs. (14). Since in molecular magnets at low temperatures both the

heat capacity and thermal conductivity strongly depend on temperature, it is more convenient to use the phonon energy  $\mathcal{E}$  as the dynamical variable instead of  $T$ , see Eq. (19). The speed of the deflagration front can be estimated if one rewrites the heat-conduction and relaxation equations in reduced forms,

$$\frac{\partial \tilde{\mathcal{E}}}{\partial \tau} = \tilde{\nabla} \cdot \tilde{\kappa} \tilde{\nabla} \tilde{\mathcal{E}} - \frac{\partial \tilde{n}}{\partial \tau}, \quad \frac{\partial \tilde{n}}{\partial \tau} = -\tilde{\Gamma}(\tilde{\mathcal{E}})\tilde{n}, \quad (80)$$

which assume full burning. The reduced variables are defined by

$$\tilde{\mathcal{E}} \equiv \frac{\mathcal{E}}{n_{-,i}\Delta E}, \quad \tau \equiv t\Gamma_f, \quad \tilde{\mathbf{r}} \equiv \frac{\mathbf{r}}{l_d}, \quad (81)$$

where  $\kappa_f$  and  $\Gamma_f$  are thermal diffusivity and relaxation rate at the flame temperature  $T_f$ , respectively, and

$$l_d = \sqrt{\frac{\kappa_f}{\Gamma_f}} \quad (82)$$

describes the width of the deflagration front. The reduced rate is

$$\tilde{\Gamma}(\tilde{\mathcal{E}}) \equiv \frac{\Gamma}{\Gamma_f} = \exp \left[ W_f \left( 1 - \frac{1}{\tilde{T}(\tilde{\mathcal{E}})} \right) \right], \quad (83)$$

where  $\tilde{\kappa} \equiv \kappa/\kappa_f$  and  $\tilde{T} \equiv T/T_f$ .

The moving flat deflagration front is a solution of Eqs. (80) that depends on the combined timelike argument

$$u \equiv \tau - \tilde{x}/\tilde{v}, \quad (84)$$

where  $\tilde{v}$  is the reduced deflagration speed. In terms of  $u$ , Eqs. (80) take the forms

$$\frac{d\tilde{\mathcal{E}}}{du} = \frac{1}{\tilde{v}^2} \frac{d}{du} \tilde{\kappa} \frac{d\tilde{\mathcal{E}}}{du} - \frac{d\tilde{n}}{du}, \quad \frac{d\tilde{n}}{du} = -\tilde{\Gamma}\tilde{n}. \quad (85)$$

They represent a nonlinear eigenvalue problem with respect to  $\tilde{v}$ . The real deflagration speed  $v$  is given by

$$v = \tilde{v} l_d \Gamma_f = \tilde{v} \sqrt{\kappa_f \Gamma_f} = \tilde{v} \sqrt{\kappa_f \Gamma_0} e^{-W_f/2}. \quad (86)$$

The advantage of using  $\tilde{\mathcal{E}}$  as a dynamical variable is that the first of Eqs. (85) can be integrated, leading to

$$\tilde{\kappa}(\tilde{\mathcal{E}}) \frac{d\tilde{\mathcal{E}}}{du} = \tilde{v}^2 (\tilde{\mathcal{E}} + \tilde{n} - 1). \quad (87)$$

Far before and far behind, the front  $\tilde{\mathcal{E}} = \text{const}$  and one recovers energy conservation, Eq. (71). One can combine Eq. (87) with the second of Eqs. (85) to eliminate  $u$ . This results in

$$\tilde{\kappa}(\tilde{\mathcal{E}}) \tilde{\Gamma}(\tilde{\mathcal{E}}) \tilde{n} \frac{d\tilde{\mathcal{E}}}{d\tilde{n}} = -\tilde{v}^2 (\tilde{\mathcal{E}} + \tilde{n} - 1) \quad (88)$$

that should be solved with the boundary conditions  $\tilde{\mathcal{E}}=0$  at  $\tilde{n}=1$  and  $\tilde{\mathcal{E}}=1$  at  $\tilde{n}=0$ .

### 1. Analytical theory

Equation (87) allows one to find the spatial variation of temperature before the front,  $u < 0$  and  $|u| \gg a$ , where  $\tilde{n} \cong 1$ . For the power-law dependences of Eqs. (15) and (17), one has  $\tilde{\kappa}(\tilde{\mathcal{E}}) = \tilde{\mathcal{E}}^{-\beta/(\alpha+1)}$ , and the solution of Eq. (87) yields the power-law asymptote before the front,  $u < 0$ ,

$$\tilde{\mathcal{E}} \cong \left[ \frac{\tilde{v}^2 \beta}{\alpha + 1} (-u + c) \right]^{-(\alpha+1)/\beta}, \quad \tilde{T} \cong \tilde{\mathcal{E}}^{1/(\alpha+1)}, \quad (89)$$

where  $c$  is the integration constant related to the position of the deflagration front. In the realistic case of  $\beta=13/3$ , the exponent in the expression for  $\tilde{T}$  is rather small. That is, the heat propagates far ahead of the deflagration front due to the divergence of thermal diffusivity at low temperature. In the case of constant  $\kappa$ , the temperature before the front decreases exponentially as one moves away from the front,

$$\tilde{\mathcal{E}} \cong e^{\tilde{v}^2 u}, \quad \tilde{T} \cong e^{\tilde{v}^2 u/(\alpha+1)}. \quad (90)$$

Here, the integration constant additive to  $u$  was set to zero. Now, one can find the variation of  $\tilde{n}$  before the front from the second of Eqs. (85) and Eq. (89) to confirm that  $1 - \tilde{n}$  is very small.

Behind the front, the  $T$  is close to the flame temperature,  $\tilde{T} \cong \tilde{\mathcal{E}} \cong 1$ , so that  $\tilde{\Gamma} \cong 1$ , and from the second of Eqs. (85), one obtains

$$\tilde{n} \cong e^{-u}. \quad (91)$$

Now, one can find the deviation  $\delta\tilde{\mathcal{E}} \equiv \tilde{\mathcal{E}} - 1$  behind the front from Eq. (87). Setting  $\tilde{\kappa}(\tilde{\mathcal{E}}) \Rightarrow 1$ , one obtains  $\partial_u \tilde{\mathcal{E}} = \tilde{v}^2 (\tilde{\mathcal{E}} + e^{-u} - 1)$  that yields

$$\tilde{\mathcal{E}} \cong 1 - \frac{\tilde{v}^2}{1 + \tilde{v}^2} e^{-u} = 1 - \frac{\tilde{v}^2}{1 + \tilde{v}^2} \tilde{n}. \quad (92)$$

This relation between  $\tilde{\mathcal{E}}$  and  $\tilde{n}$  also can be obtained from Eq. (88) with  $\tilde{\kappa}(\tilde{\mathcal{E}}) \Rightarrow 1$  and  $\tilde{\Gamma} \Rightarrow 1$  behind the front.

The speed of the deflagration front can be calculated analytically in the high-barrier limit  $W_f \gg 1$ . In this case, burning occurs in the region where the temperature is already very close to the flame temperature,  $\tilde{\mathcal{E}} \cong 1$ . Linearizing the argument of the exponential in Eq. (83) on  $\delta\tilde{\mathcal{E}} \equiv \tilde{\mathcal{E}} - 1$ , one obtains for the relaxation rate

$$\tilde{\Gamma} \cong e^y, \quad y \equiv \nu_f \delta\tilde{\mathcal{E}}, \quad (93)$$

with

$$\nu_f \equiv W_f \frac{n_{-i} \Delta E}{C_{\text{ph},f} T_f}. \quad (94)$$

The parameter  $\nu_f$  is similar to  $\nu_0$  of Eq. (25), only that it is defined with respect to the temperature  $T_f$ . Using Eqs. (15) and (73), one can simplify  $\nu_f$  to

$$\nu_f = \frac{W_f}{\alpha + 1}. \quad (95)$$

According to Eq. (79), the maximal value of  $\nu_f$  compatible with the full-burning approximation is  $\nu_{f,\text{max}} \approx 1.5$ . Nevertheless, for simplicity, we will consider the case  $\nu_f \gg 1$  within the full-burning approximation. In this case, burning occurs only when the phonon energy is very close to its final value, i.e.,  $\delta\tilde{\mathcal{E}} \sim 1/\nu_f \ll 1$ . Hence, in Eq. (87), one can make a replacement  $\tilde{\mathcal{E}} \Rightarrow 1$  and  $\tilde{\kappa}(\tilde{\mathcal{E}}) \Rightarrow 1$  in the burning region. Equation (88) then takes the form

$$\frac{dy}{d\tilde{n}} = -\nu_f \tilde{v}^2 e^{-y}. \quad (96)$$

It is convenient to consider this equation as an equation for  $\tilde{n}(y)$ . The solution satisfying the boundary conditions  $\tilde{n}=1$  before the front ( $y=-\infty$ ) and  $\tilde{n}=0$  behind the front ( $y=0$ ) reads

$$\tilde{n} = 1 - e^y. \quad (97)$$

It exists if the reduced front speed is given by  $\nu_f \tilde{v}^2 = 1$  or

$$\tilde{v} = \frac{1}{\sqrt{\nu_f}} \ll 1. \quad (98)$$

Note that this result is insensitive to the temperature dependences of the heat capacity and thermal conductivity. In real units, one obtains from Eq. (86)

$$v = \sqrt{\frac{\kappa_f \Gamma_0}{\nu_f}} e^{-W_f/2}, \quad (99)$$

where  $\nu_f$  is given by Eq. (94) or (95). Now,  $\delta\tilde{\mathcal{E}}$  can be found from the full system of equations

$$\frac{dy}{du} = \nu_f \tilde{v}^2 \tilde{n}, \quad \frac{d\tilde{n}}{du} = -e^y \tilde{n}. \quad (100)$$

With account of  $\nu_f \tilde{v}^2 = 1$  and Eq. (97), the first of these equations becomes  $\partial_u y = 1 - e^y$ . The solution is

$$y = -\ln(1 + e^{-u}). \quad (101)$$

Then, from Eq. (97), one obtains

$$\tilde{n} = \frac{1}{1 + e^u} = \frac{1}{2} \left( 1 - \tanh \frac{u}{2} \right). \quad (102)$$

The solution for  $\tilde{\mathcal{E}}$  in the whole range of  $u$  can be obtained by merging Eqs. (89) and (101). The result is

$$\tilde{\mathcal{E}} = \frac{1}{\left[ 1 + \frac{\beta}{\alpha + 1} \tilde{v}^2 \ln(1 + e^{-u}) \right]^{(\alpha+1)/\beta}} \quad (103)$$

(see Fig. 11). Its accuracy is assured by the smallness of  $\tilde{v}^2$ . In the case of  $\kappa = \text{const}$ , merging Eqs. (90) and (101) yields

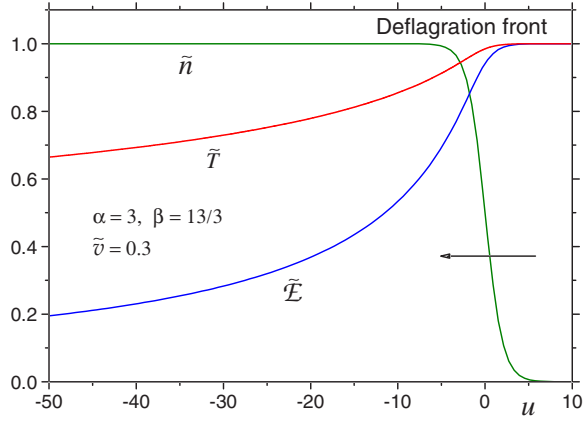


FIG. 11. (Color online) Analytical results for the deflagration front in molecular magnets in the high-barrier case,  $\tilde{v}=0.3$  (i.e.,  $\nu_f=1/\tilde{v}^2 \approx 11$ ).

$$\tilde{\mathcal{E}} = (1 + e^{-u})^{-\tilde{v}^2}, \quad (104)$$

which is the limit of  $\beta \rightarrow 0$  in Eq. (103). Note that the width of the deflagration front  $l_d$  defined by Eq. (82) is the width of the region where the magnetization changes, see Eq. (102). The width of the region where the temperature changes is  $l_d/\tilde{v} = \sqrt{\kappa_f \nu_f / \Gamma_f}$ , according to Eqs. (84) and (104). For thermal diffusivity diverging at  $T=0$  for  $\beta > 0$ , the region of the temperature variation becomes very broad and its width cannot be defined.

## 2. Numerical results for the deflagration front

If  $\nu_f$  of Eq. (94) is not large, the problem of the deflagration front cannot be solved analytically. Numerical solution uses Eq. (87) and the second of Eqs. (85). One starts in the region behind the front, with proper boundary conditions and arbitrary  $\tilde{v}$ , and solves equations numerically into the region sufficiently far ahead of the front. If the value of  $\tilde{v}$  is correct, and only in this case, the solution ahead of the front will be  $\tilde{n}=1$  and  $\tilde{\mathcal{E}}$  having the asymptotic form of Eq. (89). One finds  $\tilde{v}$  numerically from one of these conditions, with consistent results. The numerically calculated dependences of  $\tilde{v}$  on  $W_f$  are shown in Fig. 12. Surprisingly, for  $\alpha=\beta=0$  the high-barrier analytical theory works very well in the whole range of  $W_f$ .

On the contrary, the validity of the analytical theory in the realistic case of  $\alpha=3$  and  $\beta=13/3$  requires rather large  $W_f$ . One of the reasons for this is that the large- $W_f$  approximation, in fact, requires large  $\nu_f$  in Eq. (95). Nonzero exponents  $\alpha$  and  $\beta$  have the following effect on the deflagration speed. For  $\alpha > 1$ , the heat-conduction equation is written in terms of  $\tilde{\mathcal{E}}$ . The decrease of  $\tilde{\mathcal{E}}$  ahead of the front leads to the decrease of  $\tilde{T}(\tilde{\mathcal{E}}) = \tilde{\mathcal{E}}^{1/(\alpha+1)}$  that enters the relaxation rate  $\tilde{\Gamma}$ . For  $\alpha > 0$ , this temperature decrease is less essential than in the case of  $\alpha=0$ . Thus, the temperature before the front is higher and the front moves faster because of faster relaxation. The role of  $\beta > 0$  is similar. The heat diffusion in the region before the front is faster, the temperature before the front is higher, and the deflagration speed increases.

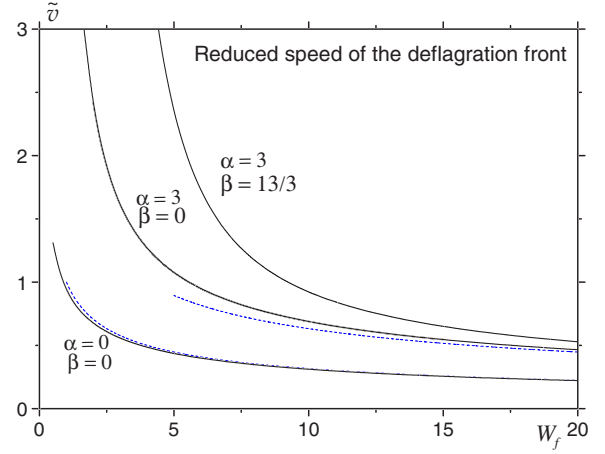


FIG. 12. (Color online) Numerical results for the reduced deflagration speed  $\tilde{v}$  vs the flame's Arrhenius exponent  $W_f$  for different temperature dependences  $C_{\text{ph}} \propto T^\alpha$  and  $\kappa \propto T^{-\beta}$ . Dashed lines are the  $W_f \gg 1$  asymptotes  $\tilde{v} \approx \sqrt{(\alpha+1)/W_f}$ .

## VII. FULL NUMERICAL SOLUTION OF THE DEFLAGRATION PROBLEM

In this section, we consider the entire process of deflagration, including ignition and front propagation, using the full system of equations describing heat transfer and relaxation. The most convenient for this purpose are Eqs. (80), since here, both  $\tilde{n}$  and  $\tilde{\mathcal{E}}$  are between 0 and 1, whereas the width of the deflagration front for  $\tilde{n}$  is of order 1. One can see that the existence of the propagating front requires  $\tilde{R} \gg 1$ . For  $C_{\text{ph}}$  given by Eq. (15), the parameter  $\delta$  of Eq. (26) becomes

$$\delta = \tilde{\Gamma}_{\text{ig}}^{(\infty)} / \tilde{\Gamma}_\kappa, \quad (105)$$

where  $\tilde{\Gamma}_\kappa = 2\tilde{\kappa}_0 / \tilde{R}^2$ ,

$$\tilde{\Gamma}_{\text{ig}}^{(\infty)} = \frac{W_f}{(\alpha+1)\tilde{T}_0^{\alpha+2}} \tilde{\Gamma}(\tilde{T}_0), \quad (106)$$

and  $\tilde{\Gamma}(\tilde{T}_0)$  is given by Eq. (83) with  $\tilde{T}(\tilde{\mathcal{E}}) \Rightarrow \tilde{T}_0$ . If  $\tilde{T}_0=1$  (i.e.,  $T_0=T_f$ ), then the ignition rate  $\tilde{\Gamma}_{\text{ig}}^{(\infty)} \sim W_f$  is very large. Thus, raising the temperature at the end of the sample up to  $T_f$  immediately ignites deflagration. If the temperature is raised up to  $T_0$  that is sufficiently lower than  $T_f$ , ignition occurs after a substantial ignition time. For illustration, below we use temperature-independent thermal diffusivity  $\kappa$ .

Theoretically, the most simple case is ignition out of the state with initially uniform temperature  $T=T_0$  and the boundary condition  $T=T_0$ . In this case, ignition should occur in the middle of the sample where the temperature rise due to the relaxation is most prominent. However, well above the ignition threshold,  $\delta \gg \delta_c$ , thermal runaway practically occurs simultaneously throughout the sample, so that there is no propagating deflagration front. The same happens in the fast-burning regime  $W_f \lesssim 1$ . The ignition in the middle followed by a front propagation to the ends can only be observed in large samples not very far above the ignition threshold. Figure 13 shows a three-dimensional plot of the metastable

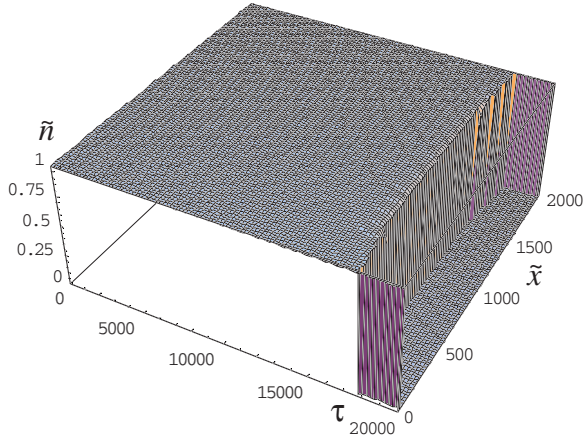


FIG. 13. (Color online) Ignition and deflagration in the uniform 1d model for  $\alpha=3$ ,  $W_f=10$ ,  $\tilde{T}_0=0.4$ , and  $\tilde{R}=1000$ .

population  $\tilde{n}(\tilde{x}, \tau)$  in the 1d model with  $\alpha=3$ ,  $W_f=10$ ,  $\tilde{T}_0=0.4$ , and  $\tilde{R}=1000$ . Here,  $\tilde{x}=0$  corresponds to the end of the sample and  $\tilde{x}=\tilde{R}$  corresponds to its center. One can see from Fig. 13 that, for the chosen set of parameters, the runaway occurs simultaneously in approximately half of the sample around its center and then the deflagration front propagates across the rest of the sample to its ends. This is more clearly seen in Fig. 14 that shows the metastable population averaged over the sample,

$$\tilde{n}_{\text{avr}}(\tau) = \frac{1}{\tilde{R}} \int_0^{\tilde{R}} d\tilde{x} \tilde{n}(\tilde{x}, \tau). \quad (107)$$

After a long plateau that determines the ignition time,  $\tilde{n}_{\text{avr}}(\tau)$  drops almost vertically but then continues down with a finite slope until it hits the horizontal axis. The region with the finite slope corresponds to the propagating front and can be made larger by decreasing  $\tilde{T}_0$  and thus decreasing  $\delta$ . This, however, drastically increases the ignition time and makes numerical calculations difficult. In general, ignition from the

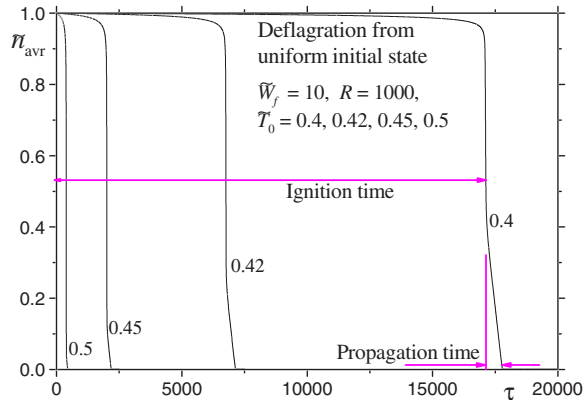


FIG. 14. (Color online) Time dependence of the average metastable population in the uniform 1d model for  $\alpha=3$ ,  $W_f=10$ ,  $\tilde{R}=1000$ , and different  $\tilde{T}_0$ .

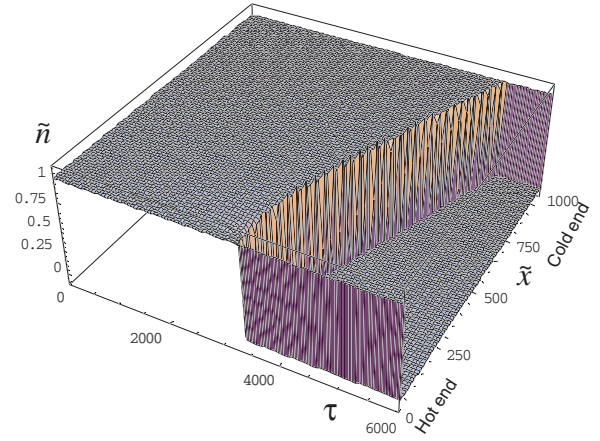


FIG. 15. (Color online) Ignition and deflagration in the 1d model with temperature gradient. The parameters are  $\alpha=3$ ,  $W_f=10$ ,  $\tilde{T}_0=0.4$ , and  $\tilde{L}=2\tilde{R}=1000$ . Initial state is the stationary state in the absence of heat release with  $T=T_0$  at the left end and  $T=0$  at the right end. Ignition occurs after the ignition time  $\tilde{\tau}_{\text{ig}} \approx 3000$  near the hot left end ( $\tilde{x}=0$ ), and then the deflagration front propagates toward the right cold end.

uniform state is not the best way to initiate deflagration. The value  $\tilde{T}_0=0.4$  is well above the ignition threshold,  $\delta/\delta_c \approx 85$ , so that one could expect the ignition rate to be the one of the infinite sample,  $\tilde{\Gamma}_{\text{ig}}^{(\infty)}$ . Equation (106) yields  $\tilde{\tau}_{\text{ig}}^{(\infty)} = 1/\tilde{\Gamma}_{\text{ig}}^{(\infty)} \approx 13\,400$ , whereas the actual ignition time is  $\tilde{\tau}_{\text{ig}}^{(\infty)} \approx 17\,200$ , see Fig. 14. The discrepancy is due to the explosive approximation  $\tilde{n} \Rightarrow 1$  made in the derivation of the formula for  $\tilde{\Gamma}_{\text{ig}}^{(\infty)}$  (see Sec. III). Decreasing of  $\tilde{n}$  during the ignition makes the heat release smaller and the ignition time longer.

Figure 15 shows the ignition and propagation of the deflagration front for the metastable population  $\tilde{n}$  in the model with temperature gradient, see Sec. IV C. Initial state is the stationary state in the absence of heat release with  $T=T_0$  at the left end and  $T=0$  at the right end. Ignition occurs after the time  $\tilde{\tau}_{\text{ig}} \approx 3000$  near the hot left end ( $\tilde{x}=0$ ), and then the deflagration front propagates toward the right cold end ( $\tilde{x}=\tilde{L}$ ). Accordingly, the time dependence of  $\tilde{n}_{\text{avr}}$  shown in Fig. 16 consists of a long plateau followed by a drop to zero after the ignition time. The slope of  $\tilde{n}_{\text{avr}}(\tau)$  in the drop region is proportional to the speed  $\tilde{v}$  of the deflagration front.

In the case of a rapid rise of the temperature up to  $T_0$  at the ends, with the initial temperature of the sample being much lower than  $T_0$ , there can be two scenarios considered in Sec. V C. Immediately above the deflagration threshold, the ignition occurs in the middle of the sample, while well above the threshold, the ignition occurs near the ends. The space-time variations  $\tilde{n}(\tilde{x}, \tau)$  and  $\tilde{T}(\tilde{x}, \tau)$  are shown in Figs. 17(a) and 17(b) in the case of symmetric temperature increase well above the ignition threshold at the ends. One can see that the two deflagration fronts meet at the center.

## VIII. DISCUSSION

So far, experimental work on magnetic deflagration has been limited to measurements of the flame speed. The pro-

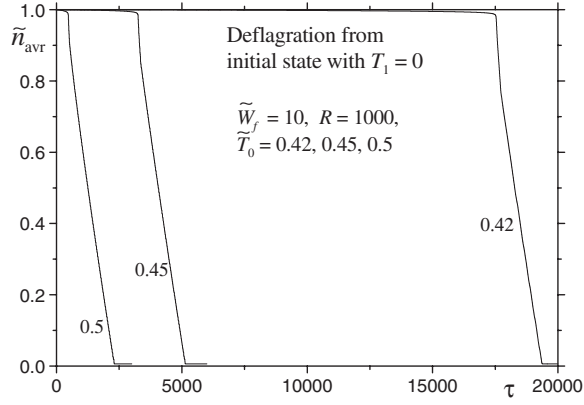


FIG. 16. Time dependence of the average metastable population  $\bar{n}$  in the  $1d$  model with temperature gradient for  $\alpha=3$ ,  $W_f=10$ ,  $\tilde{R}=1000$ , and different  $\tilde{T}_0$ . The slope of  $\bar{n}(\tau)$  at the steps is proportional to the front speed  $\tilde{v}$ .

posed theory provides the framework for more detailed experimental studies suggested in this section.

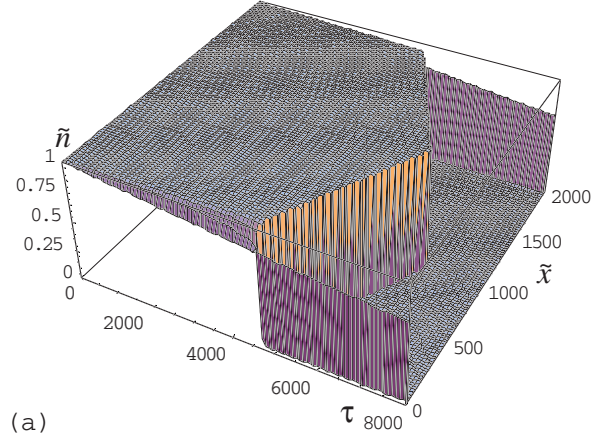
#### A. Deflagration threshold

According to the theory, the magnetic deflagration in a crystal of magnetic molecules can be ignited by increasing either magnetic field or temperature. The simplest situation is when the magnetic field and temperature of the sample boundary  $T_0$  are independent of coordinates. In this case, the crystal loses stability against formation and propagation of the flame (magnetic avalanche) when the rate of the spin flip for an individual molecule,  $\Gamma(H, T_0)$ , exceeds

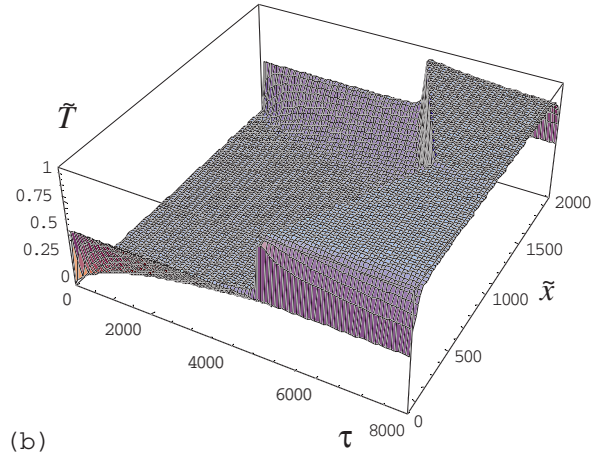
$$\Gamma_c = \frac{8k(T_0)k_B T_0^2}{U(H)\Delta E(H)n_{-,i}l^2}. \quad (108)$$

Here,  $k(T_0)$  is coefficient of thermal conductivity at  $T=T_0$ ,  $U(H)$  and  $\Delta E(H)$  are the field-dependent energy barrier and energy difference, respectively, between spin-up and spin-down states,  $l$  is some characteristic length, and  $n_{-,i}$  is the initial fraction of molecules available for burning. It can be expressed via (negative) initial magnetization  $M_i$  and the saturation magnetization  $M_0$  as  $n_{-,i}=(M_0-M_i)/(2M_0)$ . As to the parameter  $l$ , it is uniquely determined by geometry and is of order of the smallest dimension of the crystal. Equation (108) provides the dependence of the critical magnetic field on the temperature of the sample, or, inversely, the dependence of the critical temperature of the sample on the magnetic field, see Fig. 2. The deeps in  $T_0(H)$  at regularly spaced fields are due to the maxima of  $\Gamma(H, T_0)$  at tunneling resonances. Note that Eq. (108) contains explicit dependence of the deflagration threshold on the initial magnetization that should be easy to test in experiment.

Similar relations have been obtained by us in the presence of field and temperature bias, see Sec. IV. Among other things, we have demonstrated that the bias suppresses deflagration. The most important outcome of this study is the elucidation of the nature of magnetic avalanche. Contrary to the initial beliefs, the avalanche does not develop from a



(a)



(b)

FIG. 17. (Color online) (a) Variation of the metastable population  $\bar{n}$  during ignition and deflagration in the  $1d$  model with the temperature quickly raised up to  $\tilde{T}_0$  at both edges, whereas the initial temperature is zero. The parameters are  $\alpha=3$ ,  $W_f=10$ ,  $\tilde{T}_0=0.5$ , and  $\tilde{L}=2\tilde{R}=1000$ . Ignition occurs after the ignition time  $\tilde{\tau}_{\text{ig}} \approx 4500$  near the edges and then the deflagration fronts propagate toward the center and meet there. (b) Temperature variation during ignition and deflagration in the same case as above. One can see how the heat propagates into the sample, and the width of the region with elevated temperature near the edges increases.

small nucleus of the magnetization reversal inside the crystal. It begins as an instability of a smooth temperature profile when the spin-flip rate of individual molecules (the burning rate) exceeds the rate at which the heat flows out of the burning region. The effect is exponentially sensitive to the magnetic field and temperature of the sample. Even a slight fluctuation of  $H$  or  $T_0$  may take the system deep inside the instability region ( $\Gamma \gg \Gamma_c$ ), thus explaining the abrupt and sometimes unpredictable nature of the avalanche. It will be interesting to see if experiments confirm our predictions for the deflagration threshold at various initial conditions.

#### B. Ignition time

In this paper, we have addressed situations when the crystal is instantaneously brought inside the instability region. In Sec. V, we have demonstrated that the ignition of the defla-

gration occurs after a finite time elapses from the moment when the instability threshold is crossed. When crossing the threshold on field or temperature, the ignition rate changes from zero below the threshold to a some finite value above the threshold, see Figs. 7–9. The deeper one penetrates into the instability region the smaller is the ignition time. Most of the experiments on magnetic avalanches were done in a field-sweep mode, when the magnetic field changes at a constant rate,  $H=rt$ , from a large negative value to a large positive value. In this case, the field  $H'_c$  at which the avalanche occurs should be approximately determined by the equation  $H'_c=H_c+r\tau_{ig}(H'_c)$ , where  $H_c$  is the critical field at a temperature  $T_0$  plotted in Fig. 2. Since the ignition time rapidly falls as  $H$  grows above  $H_c$ , it is clear that for sufficiently small sweep rates  $r$ , the field  $H'_c$  must be very close to  $H_c$ . This condition is always fulfilled in a field-sweep experiment unless a pulse field technique is used with a very large  $r$ . Thus, a typical field-sweep experiment is capable of testing the  $H_c(T_0)$  dependence plotted in Fig. 2, but not probing the ignition time. To measure the ignition time, one should apply different techniques. The trick is to cross the stability threshold by a finite step on field or temperature during the time interval that is small compared to the ignition time. This can be achieved by using a small coil with a short time constant in addition to the large coil needed to bring the system close to the threshold. Alternatively, one can use fast heaters to cross the deflagration threshold on the temperature of the sample or on the temperature of one end of the sample along the lines of Sec. V C.

Results obtained in one dimension (Secs. V and VII) show that under symmetric conditions, the avalanche ignites in the middle of the sample or simultaneously at two symmetric regions away from the center. Symmetry arguments suggest that this should also be the case for any symmetric sample. In the meantime, experiments done under uniform field and temperature conditions often report the ignition of the deflagration persistently at one end of the sample. Explanation of this observation should be sought in the inevitable asymmetry of the heat flow inside and out of the real crystal. Such an asymmetry occurs due to the asymmetry of the crystal shape, internal inhomogeneity, or as a result of the asymmetric thermal insulation from the environment. It should lead to the asymmetric temperature profile of a quasiequilibrium state below the deflagration threshold and, thus, asymmetric ignition of the deflagration. Our studies elucidate the crucial role of the boundary conditions. This should be addressed in future experiments by studying, e.g., deflagration in thermally insulated crystals alongside with crystals that freely exchange heat with the environment and under asymmetric boundary conditions.

### C. Velocity and width of the deflagration front

Measured field and temperature dependences of the velocity of the magnetic avalanche are in a reasonably good agreement with the concept of deflagration.<sup>1,10</sup> This agreement, however, has only been established with an accuracy to the exponent, and the prefactor was estimated by orders of magnitude. In Sec. VI, we provided a more detailed study of the

developed deflagration. Our result for the speed of the deflagration front reads

$$v(H) = \sqrt{\frac{4k_B T_f \kappa(T_f) \Gamma(H, T_f)}{U(H)}}, \quad (109)$$

where  $\kappa$  is thermal diffusivity,

$$T_f = \frac{\Theta_D}{\pi} \left[ \frac{5 n_{-i} \Delta E(H)}{3 k_B \Theta_D} \right]^{1/4} \quad (110)$$

is the flame temperature (the temperature behind the front), and  $\Theta_D$  is the Debye temperature. Numerical exercise with numbers for  $Mn_{12}$  and fields used in experiment immediately shows that the above formulas give correct estimate of  $v$  and  $T_f$  and their correct field dependence. Future experiments should show whether these formulas provide quantitative description of the developed magnetic deflagration.

An interesting observation that follows from our theory is that in the developed magnetic deflagration, the width of the region where magnetization reverses is different from the width of the region inside which the temperature decays from  $T_f$  to  $T_0$ . In fact, the latter region is very broad and even difficult to define, see Fig. 11. This is a result of the divergence of thermal diffusivity at  $T \rightarrow 0$ , which makes low-temperature magnetic deflagration different from chemical deflagration. The latter has a well-defined width,  $l_d \sim \sqrt{\kappa(T_f)/\Gamma(T_f)}$ . In the magnetic case, however, this formula applies only to the width of the region where the magnetization reverses, but not to the region where the temperature changes. This may explain the reported difficulties in local measurements of the temperature during the deflagration process.

*Note added in proof.* There has been a controversy regarding whether spin tunneling maxima show in the dependence of the flame velocity on the magnetic field given by Eq. (109); see Refs. 1 and 10. We note in this connection that inhomogeneity of the local dipolar field in the moving deflagration front leads to the sweep of the total longitudinal magnetic field, even if the applied field  $H_z$  is constant. The rate of the total field change at a point in space passed by the magnetic flame can be easily as high as 1000 T/s. This is by five orders of magnitude greater than the typical rate of the field sweep used to observe quantum steps in the magnetization curve.<sup>5</sup> Thus the quantum transitions at resonance and hence tunneling maxima in the speed of the deflagration front can be wiped out or reduced. This can be understood in terms of the incoherent Landau-Zener effect; see Sec. VI of Ref. 20. Thus for the resolution of the controversy mentioned above, our theory should be combined with magnetostatics and an accurate microscopic expression for the rate of thermally-assisted tunneling; see Sec. V of Ref. 16. This will be done elsewhere.

### ACKNOWLEDGMENTS

We thank the members of the experimental groups of Myriam Sarachik and Javier Tejada for many fruitful discussions and for providing us with experimental data. This work has been supported by the NSF Grant No. EIA-0310517.

- <sup>1</sup>Y. Suzuki, M. P. Sarachik, E. M. Chudnovsky, S. McHugh, R. Gonzalez-Rubio, N. Avraham, Y. Myasoedov, E. Zeldov, H. Shtrikman, N. E. Chakov, and G. Christou, *Phys. Rev. Lett.* **95**, 147201 (2005).
- <sup>2</sup>R. Sessoli, D. Gatteschi, A. Caneschi, and M. A. Novak, *Nature (London)* **365**, 141 (1993).
- <sup>3</sup>E. M. Chudnovsky and J. Tejada, *Lectures on Magnetism* (Rinton, Princeton, 2006).
- <sup>4</sup>E. M. Chudnovsky and J. Tejada, *Macroscopic Quantum Tunneling of the Magnetic Moment* (Cambridge University Press, Cambridge, 1998).
- <sup>5</sup>J. R. Friedman, M. P. Sarachik, J. Tejada, and R. Ziolo, *Phys. Rev. Lett.* **76**, 3830 (1996).
- <sup>6</sup>J. F. Fernández and J. J. Alonso, *Phys. Rev. B* **72**, 094431 (2005).
- <sup>7</sup>F. Fominaya, J. Villain, P. Gandit, J. Chaussy, and A. Caneschi, *Phys. Rev. Lett.* **79**, 1126 (1997).
- <sup>8</sup>C. Paulsen and J.-G. Park, in *Quantum Tunneling of Magnetization—QTM'94*, edited by L. Gunther and B. Barbara (Kluwer, Dordrecht, 1995).
- <sup>9</sup>E. del Barco, J. M. Hernández, M. Sales, J. Tejada, H. Rakoto, J. M. Broto, and E. M. Chudnovsky, *Phys. Rev. B* **60**, 11898 (1999).
- <sup>10</sup>A. Hernández-Minguez, J. M. Hernández, F. Macia, A. Garcia-Santiago, J. Tejada, and P. V. Santos, *Phys. Rev. Lett.* **95**, 217205 (2005).
- <sup>11</sup>E. M. Chudnovsky and D. A. Garanin, *Phys. Rev. Lett.* **93**, 257205 (2004).
- <sup>12</sup>I. Glassman, *Combustion* (Academic, New York, 1996).
- <sup>13</sup>A. M. Gomes, M. A. Novak, R. Sessoli, A. Caneschi, and D. Gatteschi, *Phys. Rev. B* **57**, 5021 (1998).
- <sup>14</sup>A. M. Gomes, M. A. Novak, W. C. Nunes, and R. E. Rapp, *J. Magn. Magn. Mater.* **226-230**, 2015 (2001).
- <sup>15</sup>F. Fominaya, J. Villain, T. Fournier, P. Gandit, J. Chaussy, A. Fort, and A. Caneschi, *Phys. Rev. B* **59**, 519 (1999).
- <sup>16</sup>D. A. Garanin and E. M. Chudnovsky, *Phys. Rev. B* **56**, 11102 (1997).
- <sup>17</sup>J. M. Hernández, X. X. Zhang, F. Luis, J. Bartolomé, J. Tejada, and R. Ziolo, *Europhys. Lett.* **35**, 301 (1996).
- <sup>18</sup>C. Kittel, *Quantum Theory of Solids* (Wiley, New York, 1963).
- <sup>19</sup>D. A. Garanin and V. S. Lutovinov, *Ann. Phys. (N.Y.)* **218**, 293 (1992).
- <sup>20</sup>D. A. Garanin and E. M. Chudnovsky, *Phys. Rev. B* **65**, 094423 (2002).